Bulletin of Earthquake Engineering (2019) 17:603–634
https://doi.org/10.1007/s10518-018-0464-z

ORIGINAL RESEARCH

Deterministic seismic risk assessment in the city of Aigion (W. Corinth Gulf, Greece) and juxtaposition with real damage due to the 1995 *Mw*6.4 earthquake

G. Giannaraki[1] · I. Kassaras[1] · Z. Roumelioti[2] · D. Kazantzidou-Firtinidou[1] · A. Ganas[3]

Received: 29 June 2018 / Accepted: 1 September 2018 / Published online: 12 September 2018

Abstract
Earthquake scenarios were applied towards seismic risk assessment in the earthquake prone city of Aigion (W. Corinth Gulf), by combining deterministic seismic hazard and empirical structural vulnerability. Ground motions for three hazardous fault sources for Aigion were generated using a finite source stochastic simulation technique, taking into account the well-established seismotectonics of the area and site effects derived from ambient noise horizontal-to-vertical-spectral-ratios (HVSR). Validation of the parameters of the stochastic simulation and the estimated damage was performed with respect to real recordings and the damage database of a past seismic event in the area. Vulnerability was assessed empirically for an exposure model comprising 3200 buildings, compiled with on site and remoted techniques. The European Macroseismic Scale (EMS-98) was used to describe the ground motion severity in terms of macroseismic intensity and the taxonomy of the building stock into 7 structural types. Seismic risk was spatialized using GIS mapping tools on a building block scale in terms of EMS-98 damage grades and their maximum probability of occurrence. The obtained risk assessment models indicate that the northeastern and partly the southern part of Aigion are more susceptible to damage, in accordance with damage distribution from the most recent *Mw*6.4 disastrous earthquake for the city in 1995, the site amplification inferred from HVSR, and the assessed vulnerability of the constructions. Nevertheless, the current building stock demonstrates significantly enhanced seismic behaviour, due to rehabilitation after the 1995 earthquake. Despite unavoidable uncertainties, intrinsic to both the method and data, the herein seismic risk assessment appears realistic and consistent, thus allowing its exploitation towards loss estimation and mitigation scenarios.

Keywords Seismic risk · Stochastic simulation · Empirical vulnerability · HVSR · RiskUE-LM1 · Corinth Gulf

✉ I. Kassaras
kassaras@geol.uoa.gr

[1] Department of Geology and Geoenvironment, National and Kapodistrian University of Athens, 15784 Athens, Greece

[2] Department of Civil Engineering, Aristotle University of Thessaloniki, 54124 Thessaloníki, Greece

[3] Institute of Geodynamics, National Observatory of Athens, 11810 Athens, Greece

1 Introduction

The objective of this research is a comprehensive physical risk assessment in Aigion in the western Corinth Gulf, a region of high seismic hazard, capable of producing strong earthquakes of $M \geq 6$ with short recurrence periods (e.g. Papazachos and Papazachou 1997). The good knowledge of the area's seismotectonics resulted from intensive investigations in the last decades (e.g. Armijo et al. 1996; Bell et al. 2011) and the fact that new data was obtained in the frame of the ASPIS-KRIPIS (2015) research project, motivated the selection of Aigion as a candidate area for studying seismic risk. In addition, Aigion was selected considering that it is surrounded by numerous seismic stations (HUSN—http://bbnet.gein.noa.gr; CRL—http://crlab.eu; RASMON/CORSSA—http://www.corssa.gr/) which may offer real-time input ground motions in a future Rapid Risk Assessment (RRA) system that may benefit from data and results of this study.

Aigion lies in the western Corinth Gulf (Central Greece), an asymmetric graben (e.g. Doutsos and Poulimenos 1992; Hatzfeld et al. 2000; Micarelli et al. 2006) and one of the fastest deforming continental rifts globally, opening at a rate of 15 cm/year (e.g. Avallone et al. 2004). W. Corinth Gulf is formed by both onshore and offshore en-échelon E-W and SE-NW striking normal faults (e.g. Palyvos et al. 2005; Bell et al. 2011) (Fig. 1). According to the latest national building code EAK-2000 (2003), Aigion belongs to the zone of intermediate design Peak Ground Acceleration PGA = 0.24 g for a return period of 475 years. Seismicity in the area is high, with the city of Aigion and the neighboring sites having suffered from several strong earthquakes in the past. The most recent destructive earthquake in the area that caused human casualties and severe structural damage in Aigion and its surroundings, was the 15th June 1995 event of *Mw*6.4, the detailed investigation of which offered a wide range of data that comprises the basis of the current research.

The issue of seismic design in Greece falls in the jurisdiction of the Earthquake Planning and Protection Organization since 1983; the latest seismic design code is in force in Greece, with enforcement nature, since 1995. However, seismic codes treat the territory in a generic manner, using simple models of soil response and vulnerability. The former, fails to predict local effects that may be largely adverse to the constructions, while the latter neglects structural characteristics related to a region's architecture and morphology (e.g. Kassaras et al. 2015, 2018). At a global level, versatile platforms on seismic risk spatialization, e.g. CAPRA, OpenQuake, RASOR, are currently widely applied, involving modern methodologies and sophisticated data analysis tools. At present, these platforms operate with built-in modules, GMPEs (Ground Motion Predictive Equations) fragility and consequence functions, hence, output lacks site specific information, regarding hazard and vulnerability assessment, with the latter subjected to improvement every time that new damage data from real earthquakes is input (e.g. Douglas et al. 2015; Tomás et al. 2017). The need, therefore, is the application of tailored and realistic hazard and vulnerability models, taking into account updated info, which are expected to improve seismic risk assessment, useful to stakeholders for risk perception and disaster management purposes.

Initiated by the above, we elaborate a realistic and tailored physical seismic risk assessment for the city of Aigion by applying a modern, fast and cost-effective methodology that combines deterministic seismic hazard, empirical structural vulnerability and stochastically simulated ground motions from finite faults. The approach followed in this study is the RiskUE-LM1 empirical vulnerability method (Milutinovic and Trendafiloski 2003) based on the EMS-98 taxonomy (Grünthal 1998), combined with finite source stochastic simulation of ground motion, taking into account site conditions. The latter were approximated

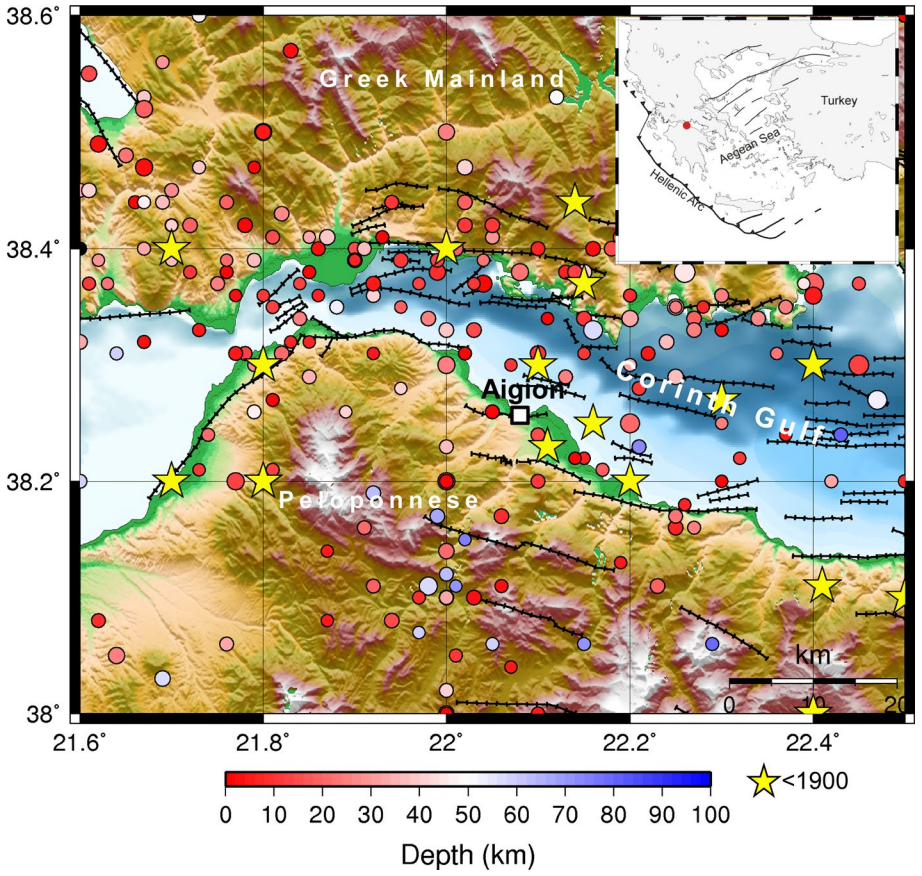

Fig. 1 Seismotectonic map of the western Corinth Gulf presenting active faults (barbed lines, Ganas et al. 2013) and epicenters of historical (yellow stars, Papazachos and Papazachou 1997) and instrumental earthquakes of M ≥ 4 (color circles, Makropoulos et al. 2012). The embedded map in the upper right corner indicates the position of Aigion city within the broader Aegean area

by Horizontal-to-Vertical-Spectral Ratios (HVSR) from free-field ambient noise measurements following the Nakamura's approach (Nakamura 1989).

Not all hazards have been covered in the presented models, i.e. surface rupture and secondary effects, such as ground failures, soil spreading, liquefaction, tsunami, etc., documented from past earthquakes. Moreover, indirect effects, which involve human safety, economic loss and societal disruption, have not been addressed, since these tasks are not within the purpose of this work. In this respect, development of complex multi-hazard scenarios, simultaneous or sequential, involving direct and indirect losses should be examined in the future.

This work is organized as following. At first, the deterministic seismic hazard assessment is performed which involves a stochastic approach for the computation of synthetic ground motions for two major historical events and a future earthquake with *Mw*6.0 on a normal fault underlying the coastal area of the city using ambient noise HVSR as proxies of site effects. The construction of the exposure model and the corresponding vulnerability estimation for the selected methodology is also discussed. The risk assessment outcome for

the three scenarios is presented in terms of EMS-98 damage grades with the highest probability of occurrence. Furthermore, we compare the outcome risk model for the city with the real damage produced due to the most recent disastrous earthquake of 1995, *Mw*6.4. Lastly, we discuss the perspectives of the outcome towards risk reduction. The flow chart of Fig. 2 illustrates the organization of this work regarding exploited data, applied methods, obtained results and future perspectives.

2 Deterministic seismic hazard analysis (DSHA)

Site-specific synthetic strong ground motions in the target area were obtained by deterministic seismic hazard analysis (DSHA), considering a set of hazardous seismic sources located close to Aigion. The stochastic finite-fault method was applied, as it was implemented in the EXSIM code (Motazedian and Atkinson 2005) and was later modified by Boore (2009). In this context, the seismic source is approximated by a rectangular fault plane, divided into discrete sub-faults, each of which is considered as a point source of an ω-squared high-frequency cut-off spectrum (Brune 1970). In the procedure, the rupture

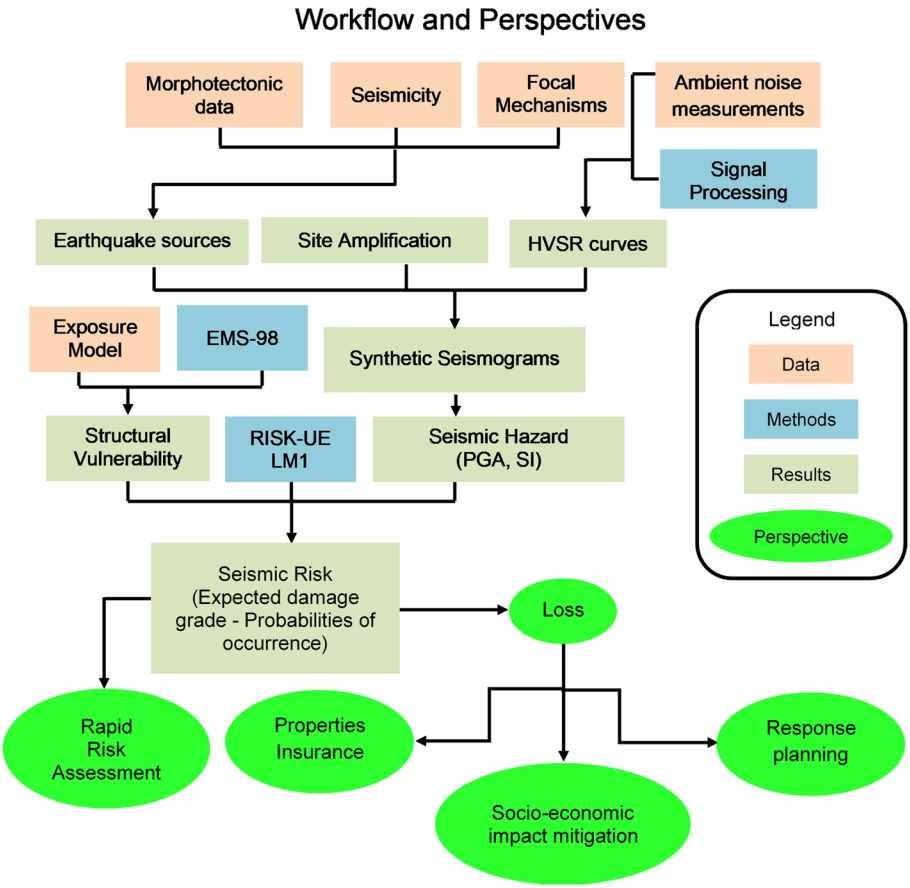

Fig. 2 Flow chart outlining the organization and the future perspectives of this study

begins on a given subfault and propagates radially with a constant velocity, triggering the neighboring subfaults until the whole fault surface is activated. The procedure was performed by considering uniform slip on the fault plane, since a variable slip model has not been published for the area. In this respect, near-source effects that are likely to occur in the target site in case of a strong earthquake were not treated in particular, since the stochastic method does not cope with low frequency pulses, therefore a deterministic simulation approach is required. Even though the latter is not within the scope of this work, which is restricted in the higher frequency band of engineering interest (1–20 Hz) given that the majority of the building stock in Aigion is characterized by low to medium-rise buildings. Nonetheless, simulating the low frequency wavefield is a stimulating future task when more and better quality data becomes available. Empirical attenuation relations were implemented to account for path effects. Ambient noise HVSR (Nakamura 1989), an alternative to costly geophysical and geotechnical methods to characterize the site response, was applied as the frequency-dependent proxy of the transfer function of the site's soil column. The one-component generic synthetic horizontal acceleration was then produced at selected positions by summing the ground motions of all sub-faults applying a proper time delay.

2.1 Parameterization of the stochastic model: validation

Prior to the implementation of the stochastic scheme, several parameters had to be empirically constrained towards generating realistic synthetic ground motions. To this aim, three past local events were stochastically simulated and several empirical parameters were tested to validate their values in order to be used in subsequent, "blind" simulations of the earthquake scenarios.

The geometry of the three "validation" fault sources (events' ID 1–3) implemented for the parameterization of the stochastic model was considered according to Table 1 and is illustrated in Fig. 3. Events 1 and 2 were recorded at the permanent accelerometric station AIGA (Fig. 6a), operated by the Geodynamics Institute-National Observatory of Athens (GI-NOA), and event 3 was recorded at station AIG2 (also in Fig. 6a), operated by the Institute of Engineering Seismology and Earthquake Engineering (EPPO-ITSAK).

The input planar fault models were discretized into certain subfaults as proposed by Beresnev and Atkinson (1999), with the slip distribution assumed to be random. Stress parameter was set equal to 56 bars after Margaris and Boore (1998), a representative value determined over several strong Greek earthquakes, the crustal shear wave velocity, $Vs = 3.4$ km/s, and the crustal density at the source depth, $rho = 2.7$ g/cm^3. Geometrical spreading $1/R$ was applied, where R is the hypocentral distance. A mean frequency-dependent quality factor that is in good agreement with local conditions in the Greek region (Hatzidimitriou 1993, 1995), $Q(f) = 275 \cdot (f/0.1)^{-2.0}$ for $f \leq 0.2$ Hz, $Q(f) = 88 \cdot f^{+0.9}$ for $f \geq 0.6$ Hz and $Q(f)$ determined from a power-law fit for $0.2 < f < 0.6$ Hz (Boore 1984, 1996), where f is the frequency, was considered to account for the S-wave anelastic attenuation. Near-surface attenuation, controlled by the high-frequency spectral decay factor kappa, κ_0, was considered equal to 0.035 s, as suggested by Margaris and Boore (1998) for rock site conditions in Greece befitting to Aigion.

The source duration, T_0 (1 s, 5 s and 0.9 s for the events 1, 2, 3 in Table 1, respectively), was estimated based on the lowest corner frequency (f_A) of the source spectrum according to the relationship of Boatwright and Choy (1992) for $4 \leq M \leq 7$, as suggested by Atkinson and Boore (1995). The distance-dependent path duration, T_P (5 s, 2.5 s and

Table 1 Description of the geometry of the fault models employed in the stochastic simulations

Event ID	Examined event	Fault	*Mw*	Strike (°)	Dip (°)	Rake (°)	Length/width (km)	Upper edge (km)	References
1	17/05/1990	–	5.2	248[b]	30[b]	− 117[b]	3.6/3.5[a] 3 × 2 subfaults	4.5	ESD
2	15/06/1995	Offshore	6.4	275	35	− 83	22/13[a] 5 × 5 subfaults	2.5	Bernard et al. (1997)
3	07/11/2014	Offshore	5.0	248	30	− 117	2.7/2.8[a] 3 × 4 subfaults	4.5	GI-NOA[c]
4	26/12/1861	East Heliki Fault (EHF)	6.7	287 (3)	60 (3)	− 78 (1)	23/15 (2) 5 × 5 subfaults	0	(1) Papazachos and Papazachou (1997) (2) McNeill et al. (2005) (3) Chouliaras et al. (2015)
5	–	Aigion Fault (AF)	6.0	270 (4,5)	60 (2,3,4,5)	− 83 (1,4)	10 (2,3)/12 (2) 4 × 6 subfaults	0.5	Bernard et al. (1997 (1), 2006 (2)) (3) McNeill et al. (2007) (4) Godano et al. (2014) (5) Chouliaras et al. (2015)

[a]Wells and Coppersmith (1994)

[b]Focal mechanism was considered similar to the one of the equivalent magnitude event 3

[c]Papaioannou (2014)

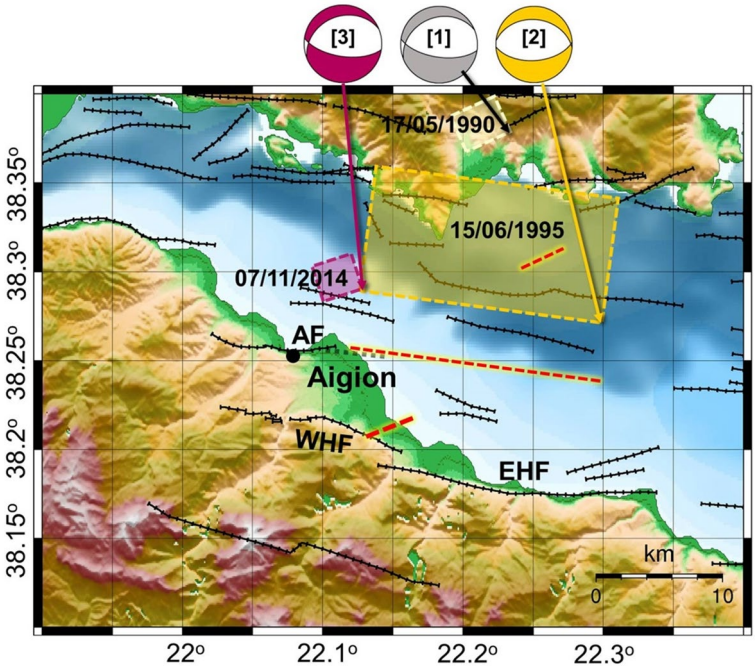

Fig. 3 Map presenting the surface projection of the fault sources (semi-transparent rectangles) of the events employed for the validation of the stochastic method. Beachballs indicate the events' focal mechanisms. Numbers within beachballs denote the events ids (see Table 1). Arrows point at the upper edge of the faults. AF: Aigion Fault. WHF/EHF: West/East Heliki Fault, and dashed red lines indicate the hypothetical surface trace of the fault models

11.1 s, respectively), was determined by subtracting T_0 from the total duration (T) of the observed records. Calculating the distance from the centroid depth (considered equivalent to the hypocentral distance), the term T_P was modelled as a single line of slope b (Boore and Atkinson 1987; Atkinson and Boore 1990, 1995). Thereby, b was calculated for each simulated event 0.15, 0.14 and 1.2, respectively, and a best-fit path duration model was obtained. Site amplification was approximated by the HVSR curves of each event (Nakamura 1989; SESAME 2005) from the respective recordings at AIGA and AIG2. The horizontal synthetic time histories, Fourier and spectral acceleration for each past event were then derived over 30 random point source simulations implemented by the SMSIM conceptual model (Boore 1996), included in EXSIM. Figure 4 presents the comparison between the output synthetic horizontal acceleration time histories and amplitude Fourier spectra with the respective observed ones for each event.

The simulation procedure yielded ground motions close to the real observations both in the time and frequency domain, especially in the higher frequency range of engineering interest (Fig. 4). The simulated PGAs, i.e. 137 cm/s^2, 504 cm/s^2 and 106 cm/s^2 for events 1, 2, 3, respectively, were found to be close to the levels of the recorded average horizontal values in all three cases, i.e. 155 cm/s^2, 500 cm/s^2 and 109 cm/s^2. It is worth noting that although the synthetic time histories slightly overestimate the duration of the recorded ones, the agreement is quite satisfactory. Taking into account the simplifications

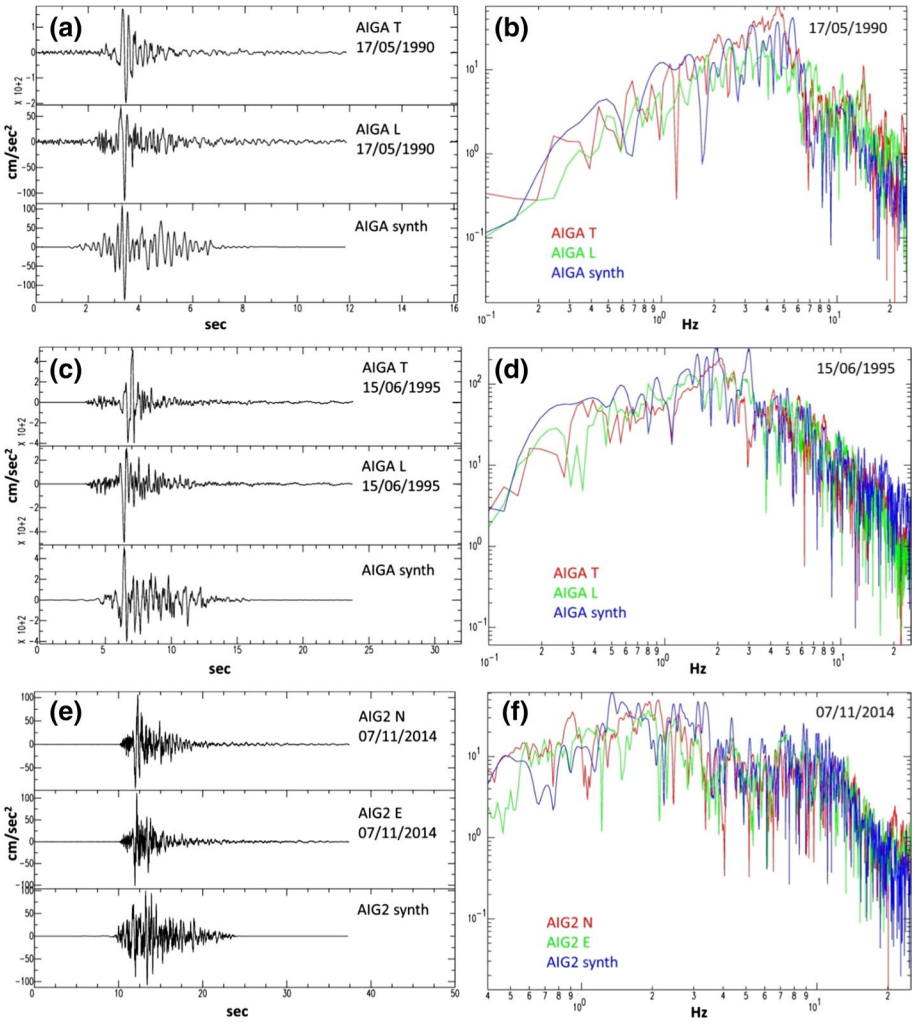

Fig. 4 Comparison between the observed horizontal acceleration time history recordings (**a**, **c**, **e**) at the AIGA (data from ESD) and AIG2 (data from EPPO-ITSAK) station and respective Fourier spectra (**b**, **d**, **f**), with the corresponding synthetics for the events 1–3 in Table 1

involved in the simulation procedure, the derived parameterization of our stochastic model is in overall satisfactory and is, thus, considered feasible for the subsequent risk analysis.

2.2 Simulation of scenario earthquakes

The validated input parameters of the stochastic simulation were used in the subsequent step of our analyses, i.e., the generation of scenario shakemaps for three hazardous fault sources close to Aigion (Table 2 and Fig. 5) (events 2, 4, and 5 in Table 1), namely the 1995 earthquake of *Mw*6.4 on an offshore low-angle normal fault (Bernard et al. 1997), the 1861 historical earthquake of *Mw*6.7 on the East Heliki Fault (EHF) (Schmidt 1879), and an earthquake

Table 2 Basic empirical input parameters employed in the EXSIM stochastic simulation

Parameter	Symbol (units)	Value	
Stress parameter	*Stress* (bars)	56	
Hypocenter location in along and down dip distance from the fault	i_0, j_0 (km)	Event ID	2 Random
			4 Random
			5 5 km, 7 km
Crustal shear-wave velocity	*Vs* (km/s)	3.4	
Crustal density at source depth	ρ (g/cm^3)	2.7	
Geometric spreading as a function of distance *R* (km)	km^{-1}	1/*R*	
Anelastic attenuation model, $Q(f)=Q_0\cdot(f)^n\, f\geq 0.6$	Q_0, η	88, 0.9	
Kappa	κ_0 (s)	0.035	
Slip distribution model	–	Event ID	2 Random
			4 Random
			5 Unity

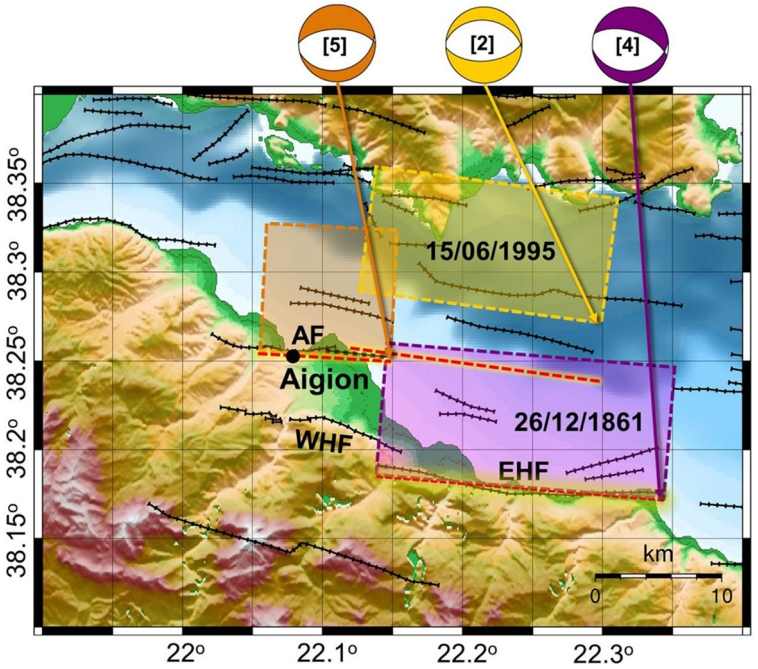

Fig. 5 Map presenting the surface projection of the fault models (semi-transparent rectangles) of the scenario earthquakes. Beachballs indicate the events' focal mechanisms. Numbers within beachballs denote the events IDs (see Table 1). Arrows point at the upper edge of the faults. AF: Aigion Fault. WHF/EHF: West/East Heliki Fault, and dashed red lines indicate the hypothetical surface trace of the fault models

of *Mw*6.0 on the Aigion Fault (AF), underlying the coastal part of the city. It should be noted that for events 2 and 4 (Table 1) the procedure was based on 30 random simulations that yielded an average PGA at each position, while for event 5, a single seed was produced (see Table 2), due to biases likely related to the very short distance of the fault.

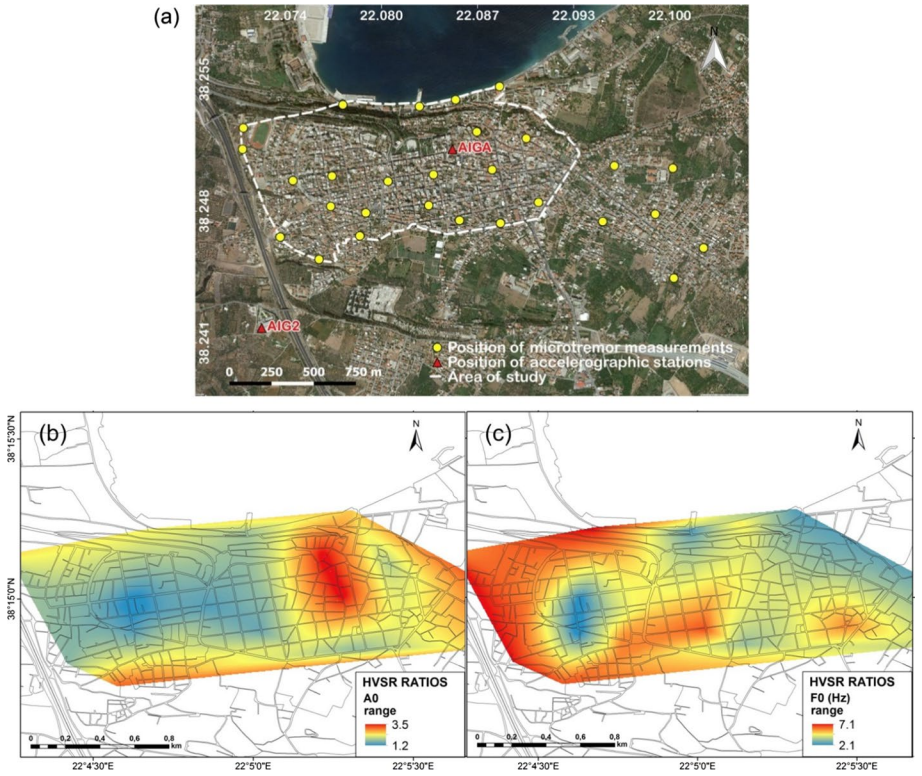

Fig. 6 **a** Position of ambient noise measurements in Aigion over Google Earth. The white dashed contour surrounds the studied area; AIGA (National Observatory of Athens) and AIG2 (Institute of Engineering Seismology and Earthquake Engineering) denote the location of accelerometric stations whose recordings were exploited to the validation procedure of the simulated model, **b** spatial distribution of ambient noise HVSR amplification factor (A_0), **c** fundamental frequency (F_0)

To incorporate the site-effect at the scale of the city of interest, we made use of free-field ambient noise measurements that have been performed in 2015 at 28 selected positions in the city of Aigion in the frame of the ASPIS-KRIPIS project (2015) (Fig. 6a). Three-component ambient noise recordings of about 30 min duration were processed using the GEOPSY software (SESAME 2005) in a broad range of engineering interest (0.2–20 Hz). For the part of the city on which we focus (Fig. 6a), the HVSR estimates exhibit amplification factors between 1.2 and 3.5 (Fig. 6b), with largest amplification inferred for the south-eastern and the central part of Aigion, and dominant frequencies between 2.1 and 7.1 Hz (Fig. 6c).

The application of ambient noise HVSRs has proven widely to reasonably represent the frequency response of the soil (e.g. Konno and Ohmachi 1998), however it has been found to underestimate a site's amplification (e.g. Bonnefoy-Claudet et al. 2006). Several experimental studies though showed that a satisfactory correlation exists between the HVSR peak and the site amplification (e.g. Rodriguez and Midorikawa 2002).The consistency of the herein ambient noise HVSR has been validated by juxtaposition with results obtained in Aigion by Apostolidis et al. (2006) and Voulgaris et al. (2010), regarding Standard Spectral Ratios (SSR) and HVSR from earthquake recordings from a

downhole array (CORSSA, www.corssa.gr), respectively. As expected, the comparison revealed an overall agreement regarding the frequencies distribution, while the ambient noise HVSR amplification was found somewhat lower, however this discrepancy is not considered critical when neglecting source directivity and soil non-linearity, as in our case.

Horizontal synthetic acceleration waveforms, randomly oriented, were computed at the microtremor locations depicted in Fig. 6a. The derived HVSR for those sites were incorporated to empirically amplify the synthetic spectra and, thus, to incorporate the site effect. Synthetic Peak Ground Acceleration (PGA) values were then used to generate a shakemap for each earthquake scenario (Fig. 7), and were further converted to Seismic Intensity (SI) through the empirical relationship of Tselentis and Danciu (2008):

$$SI(MMI) = 3.563 \cdot \log(PGA) - 0.946 \quad (1)$$

where MMI is the Modified Mercalli Intensity, considered equivalent to the EMS-98 for the description of the same effects (Musson et al. 2010). It should be noted though that the inherent uncertainties of Eq. (1) related to the statistical variability of the input data, i.e. lack of recordings, subjectivity of the observations, inclusion of soil effects, etc., (Tselentis and Danciu 2008), are acknowledged herein. However, real data from Aigion were applied

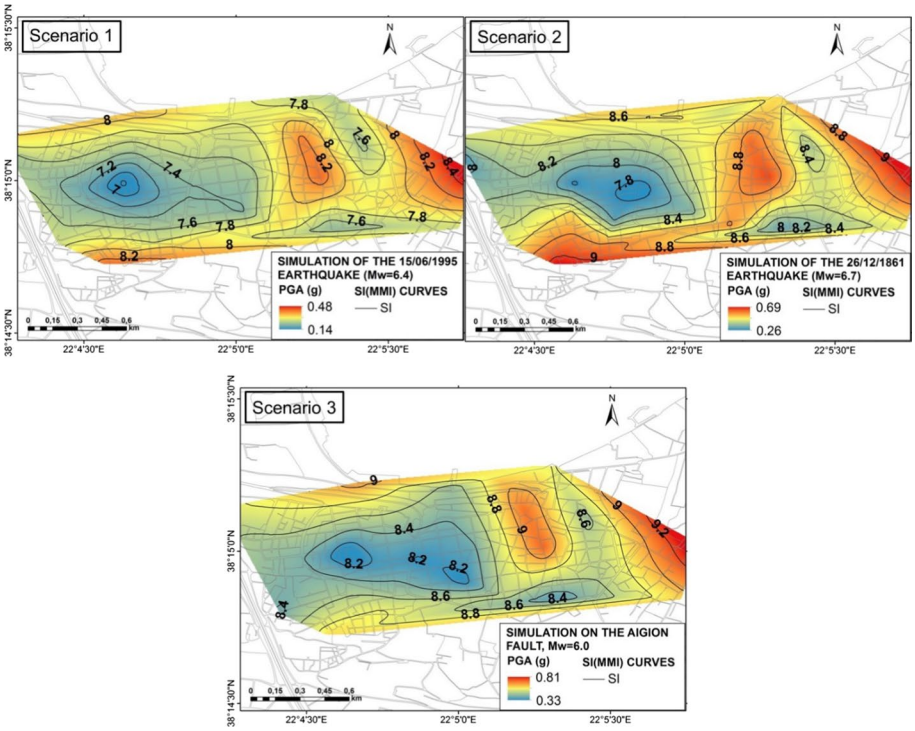

Fig. 7 Shakemaps for the city of Aigion for the three simulated earthquake scenarios (Scenarios 1–3; described in the main text). The color represents synthetic horizontal PGA, while contours correspond to discrete values of MMI

for the extraction of Eq. (1) on the one hand, and on the other it yields consistent MMI for the 1995 earthquake with existing studies (Papazachos and Papazachou 1997; Papazachos et al. 1997; Lekidis et al. 1999). Therefore we consider its implementation herein reliable.

2.2.1 Scenario 1: Repetition of the 15th June 1995 earthquake (*Mw*6.4)

The 1995 event was one of the largest and most destructive earthquakes that occurred in Greece over the past few decades. The mainshock, felt with MMI = VIII in Aigion (Lekidis et al. 1999), and its largest aftershock a few minutes later, caused 26 casualties, 200 injuries, major damage to 2000 buildings and three collapses in the city and its surroundings (Papazachos and Papazachou 1997). Secondary phenomena such as ground cracks, liquefaction, and morphological changes of the shoreline occurred both in the north and the southern coast of the gulf. Horizontal PGA exceeded 0.5 g at epicentral distance of about 16 km (AIGA station), attributed to source directivity and local conditions including soil response and topographic effects (Lekidis et al. 1999; Mavroeidis et al. 2018). Spectral acceleration of the earthquake was adverse mainly for the high buildings of the city, exhibiting values exceeding design spectra for periods T = 0.4–0.6 s (Lekidis et al. 1999). The fault model that we adopted to simulate strong ground motion from a scenario where the 1995 earthquake repeats is depicted in Fig. 5 (yellow rectangular corresponds to the surface projection of the fault model). The geometry of the adopted fault model is described in Table 1 (event ID 2), while the rest of the input parameters are listed in Table 2.

Highest PGA values (Fig. 7) were derived mainly for the southeastern and partly for the center of the city. Synthetic PGAs near the AIGA station are ~ 0.4 g, a value that is not as high as the one recorded at the same site during the 1995 earthquake. This is, most probably, because we simulated an event similar to the 1995 one (same location, magnitude, ruptured area) but without taking into account the details of the 1995 rupture, i.e. the slip distribution. When excluding edge effects, i.e. artifacts produced by the interpolation procedure, when a large distance occurs between observational points lying at the border of the map, the respective values of SI curves in the study area (see Fig. 6a) range from 6.8 to 8.2 (Fig. 7), in consistency with the observed intensities from the 1995 earthquake (e.g. Lekidis et al. 1999; Papazachos et al. 1997).

2.2.2 Scenario 2: Repetition of the 26th December 1861 earthquake with *Mw*6.7 on the East Heliki Fault (EHF)

This offshore earthquake is reckoned to be the largest in the area of Aigion after the 18th century (e.g. Albini et al. 2017). Aigion is located in the hangingwall area of the east–west striking, north-dipping Heliki normal fault. The effects of the event were catastrophic, reaching a maximum MMI = X in Aigion (Papazachos and Papazachou 1997). It caused 20 casualties and several injuries. Almost all houses in Aigion suffered serious damage and one collapsed by the strong mainshock and its largest aftershock. Intense environmental effects occurred, among which a tsunami with a run-up of 1.8 m (Papadopoulos 2003). The surface rupture (Schmidt 1879) and paleoseismological evidence (McNeill et al. 2005) indicate that the 1861 earthquake occurred on the EHF.

The fault model that we adopted to simulate ground motions for the 1861 earthquake scenario is shown in Fig. 5 (magenta rectangular corresponds to the surface projection of the fault model). The values of the input parameters are summarized in Tables 1 and 2 (event ID 4). Highest PGA values are observed mainly in the southeastern and partly in

the center of the city, consistently with the distribution of the HVSR amplification factors (Fig. 6b). The deduced SI curves (Fig. 7) range from 7.8 to the west of the center to 8.8 to the east and south of the study area (see Fig. 6a), in good agreement with the macroseismic effects of the event (Shebalin 1974; Papazachos et al. 1997).

2.2.3 Scenario 3: An earthquake with *Mw*6.0 on the Aigion Fault (AF)

The AF is one of the youngest significant normal faults in the Gulf of Corinth that is suggested to have been rapidly developed within the last 200–300 Ka, presenting a high slip rate and a total fault length of about 10 km (McNeill et al. 2007), capable of producing a *Mw*6.0 earthquake according to the empirical relations of Wells and Coppersmith (1994). Although it appears segmented along its trace and it exhibits an immature displacement profile (McNeill et al. 2007), this fault is considerably hazardous for the city of Aigion, which is mostly situated on its footwall. Historical earthquakes with destructive effects, i.e. the 14/05/1748 of $Mw = 6.6$, the 23/08/1817 of $Mw = 6.6$ and the 09/09/1888 of *Mw*6.3, all three events with MMI = IX, are likely to have ruptured the AF (Papazachos and Papazachou 1997; Pantosti et al. 2004; Bernard et al. 2006).

The fault model adopted to simulate a future earthquake on the AF is depicted in Fig. 5 (orange rectangular corresponds to the surface projection of the fault model). Due to the proximity of the specific fault model to our target area and to avoid extreme ground motions related to large slip patches in random slip distributions, we preferred for this scenario to adopt a uniform slip distribution model. All other input parameters were as previously described and as listed in Tables 1 and 2 for event ID 5.This scenario presents the highest ground motions with respect to the other scenarios. Synthetic SI curves (Fig. 7) range from 8.2 to 9 in the study area shown in Fig. 6a.

3 Exposure model and empirical vulnerability assessment

Seismic vulnerability in Aigion was assessed using the empirical RiskUE-LM1 approach (Milutinovic and Trendafiloski 2003) initially proposed by Giovinazzi and Lagomarsino 2004). The method introduces vulnerability classification of buildings by the application of Building Typology Matrices and Fuzzy Set Theory for the definition of probable discrete Vulnerability Index (VI) ranges per EMS-98 qualitative Vulnerability Classes (VCs).

The exposure model of Aigion (as per 2016, EXP-2016 hereafter) was based on the EPANTYK research project (EPANTYK 2009), which employed the Hellenic Statistical Authority (EL.STAT.) census database, while the 1995 post-seismic survey of Fardis et al. (1999) was also considered. In 2016, the initial dataset was updated and appropriately modified to represent the current building stock of Aigion on a building-by-building level. This was accomplished by two in situ surveys we conducted in most of the Aigion city area and by the use of satellite navigation (public) tools. It should be noted that monumental buildings and buildings of public use are excluded from this study since variable structural criteria are required, which are not included in the empirical method.

EXP-2016 consists of 3216 buildings belonging to 223 blocks. Out of the fifteen building typologies included in the EMS-98 taxonomy (Grünthal 1998), seven types were identified in Aigion; four types of UnReinforced Masonry (URM) and three types of Reinforced Concrete (RC) frames (Fig. 8, Table 3). Classification of the RC buildings was according to the evolution of the Greek Seismic design Codes (GSCs) (Table 3, Fig. 9), while a

Fig. 8 Examples of the 7 building typologies found in Aigion

Table 3 Building typologies in Aigion and the respective EMS-98 Vulnerability Class (VC)

Typology	Building type description	Most probable VC (EMS-98)
UnReinforced masonry (URM)		
M2	Adobe	A
M3	Simple stone	B
M5	Unreinforced masonry (bricks) Period of construction before 1970	B
M6	Unreinforced masonry (bricks) with RC floors Period of construction after 1970	C
Reinforced concrete (RC)		
RC1	Frame in RC without Earthquake Resistance Design (ERD) Period of construction: < 1959	C
RC2	Frame in RC with moderate ERD Period of construction: (1959–1995)	D
RC3	Frame in RC with high ERD Period of construction: > 1995	E

proportion of mixed URM that was observed (~ 7.3% of the total inspection), was classified according to the most vulnerable constituent material. EXP-2016 consists mainly of buildings of residential and commercial use, either exclusive or mixed, from which more than 70% are RC constructions being erected during 1970–1980 and after the disastrous earthquake of 1995. It is worth mentioning that many old masonry buildings (M2 and M3

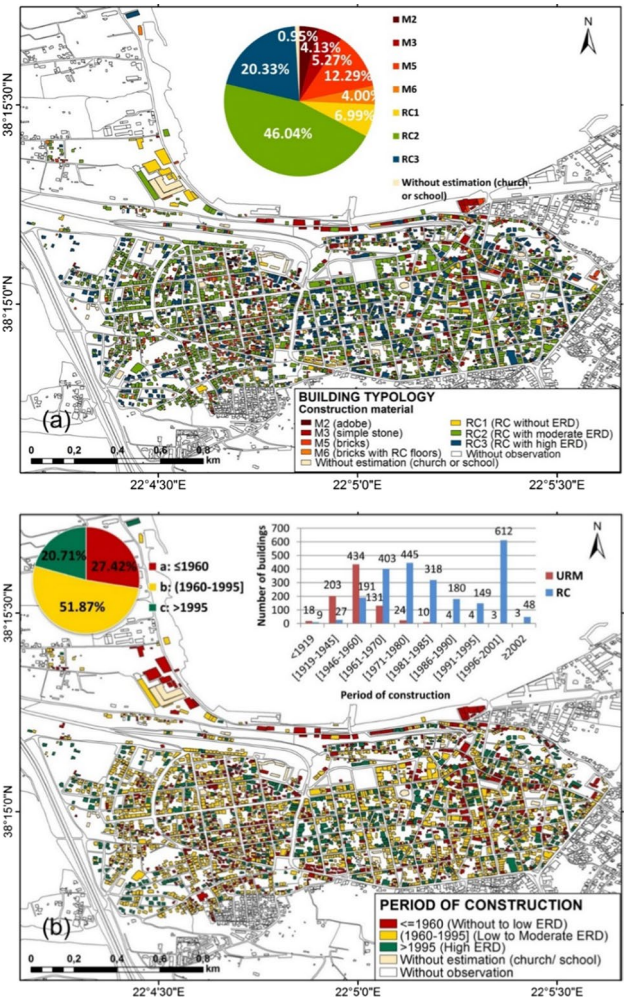

Fig. 9 The EXP-2016 model with respect to: **a** the construction material; **b** the period of construction. Percentages are shown in the embedded pie-charts. The embedded histogram shows the number of buildings per construction period

types), damaged in 1995, were demolished or abandoned, explaining their low multitude nowadays.

Based on the identified typology, each inspected building was then assigned the most probable Vulnerability Class (VC) according to the generic EMS-98 taxonomy scheme (Grünthal 1998) (Table 3, Figs. 9a, 10). The major part of the city's building stock (> 66%) was found to be of moderate to low vulnerability (VC = D and VC = E), having being built according to the first (Greek government gazette 160/A 1959; and its 1984 revision) and more rigorous (EAK-2000 2003) provisions of the GSCs, respectively. The most vulnerable buildings (VC = A and VC = B) of the URM typologies compose of ~ 22% of the exposed assets, while the most recent type of M6 is the less vulnerable among them due to the assumed addition of well-connected RC floor-slabs, which allow for an enhanced, box-like behaviour.

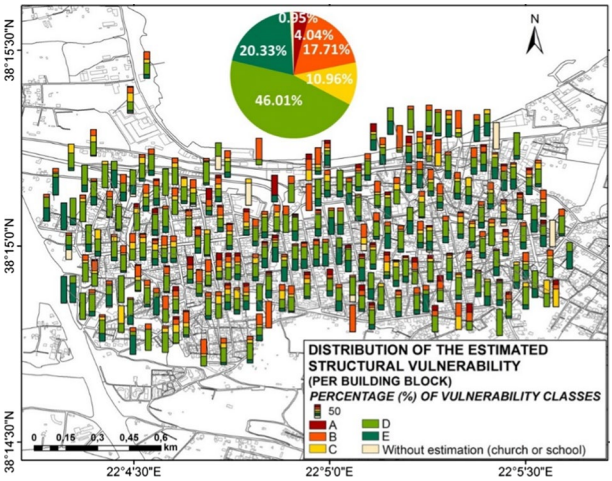

Fig. 10 Vulnerability estimation per building block in Aigion according to EMS-98 and the corresponding percentage of each Vulnerability Class VC (embedded pie-chart)

Thereinafter, each inspected building was assigned the most probable typological VI (V_I*) as per Giovinazzi and Lagomarsino (2004) (Table 4). V_I* was subsequently increased or decreased according to modifier scores (V_{mk}), accounting for structural and morphological peculiarities (Giovinazzi and Lagomarsino 2004). The Total Vulnerability Index $\bar{V}_I$ for a building was then obtained as: $\bar{V}_I = V_I^* + \Delta V_m$, where the term ΔV_m (total modifier index) corresponds to the algebraic summation of all V_{mk}. It is worth noting that ΔV_m is constrained empirically and thus, it may also include V_{mk} which account for regional characteristics related to the local architecture and/or topography. Table 4 outlines the contribution of structural characteristics of the Aigion buildings to the ΔV_m per typology, after expert's judgment.

In summary, the following could be pointed out with regard to the characteristics of the exposed assets of the target area:

- About 80% of the inspected buildings was found to be well-maintained.
- Most of the buildings are low-rise with a maximum of two storeys (87.5%).
- Almost 37% of the city's building stock appears to be vertically irregular.
- About 80% of buildings were found regular in plan.
- Regarding the position of the buildings in relation to their adjacent constructions, about 30% were independent.
- About 47% of URM buildings may be adversely affected by roof weight.
- In some cases, buildings' vulnerability was jeopardized by adjacent buildings of different height (~27% of the URM) and staggered floors (~33% of the total sample).
- Positive interventions were observed in several URM constructions which are assumed to have enhanced their seismic performance.

The applied approach (Giovinazzi and Lagomarsino 2004) enabled a numerical scale that ranges from 0 (best) to 1 (worst) vulnerability, in substitution of the EMS-98 VC attributes. The concluded percentage of $\bar{V}_I$ per inspected building in Aigion is indicated in the embedded pie-chart of Fig. 11a, in which the derived average $\bar{V}_I$ per building block is also mapped. The average $\bar{V}_I$ per building block ranges from ~0.3 to ~0.74, with the majority of the building stock exhibiting $\bar{V}_I$=0.5–0.6 (~36%). The most vulnerable buildings

Table 4 Scores of the typological indices (V_I*) and behaviour modifiers (V_{mk}) applied to Aigion, according to Giovinazzi and Lagomarsino (2004) and the herein modifications accounting for regional characteristics, marked as [(2)]

Behavior modifiers	Attributes	URM			RC		
		M2	M3, M5	M6	RC1	RC2	RC3
		V_I*					
		0.84	0.74	0.616	0.644	0.484	0.324
		V_{mk}					
State of preservation	Good	−0.04	–	–	–		
	Bad	+0.04	+0.04	+0.02	0		
Number of floors	Low: [0–2][a]; [0–3][b]	−0.08	−0.02	−0.02	−0.02		
	High: ≥ 6[a]; ≥ 8[b]	+0.08	+0.04	+0.04	+0.04		
Plan irregularity	Geometry	+0.04	+0.04	+0.02	0		
Vertical irregularity	Geometry/Mass distribution	+0.04	+0.04	+0.02	0		
Roof	Weight, thrust and connections	+0.04	–	–	–		
Retrofitting intervention	Good	−0.04 [(2)]	–	–	–		
	Bad	+0.04 [(2)]					
Aggregate building: position	Middle	−0.04	–	–	–		
	Corner	+0.04					
	Header	+0.06					
	Adjacent	–	+0.04	+0.04 [(2)]	0		
Aggregate building: elevation	Staggered floors	+0.04	+0.04 [(2)]	+0.04 [(2)]	0		
	Buildings with different height (for the lower building)	+0.02 [(2)] (header)	–	–	–		
		+0.04 [(2)] (middle)					
Short-column	Existence	–	+0.02	+0.01	0		

[a]URM

[b]RC

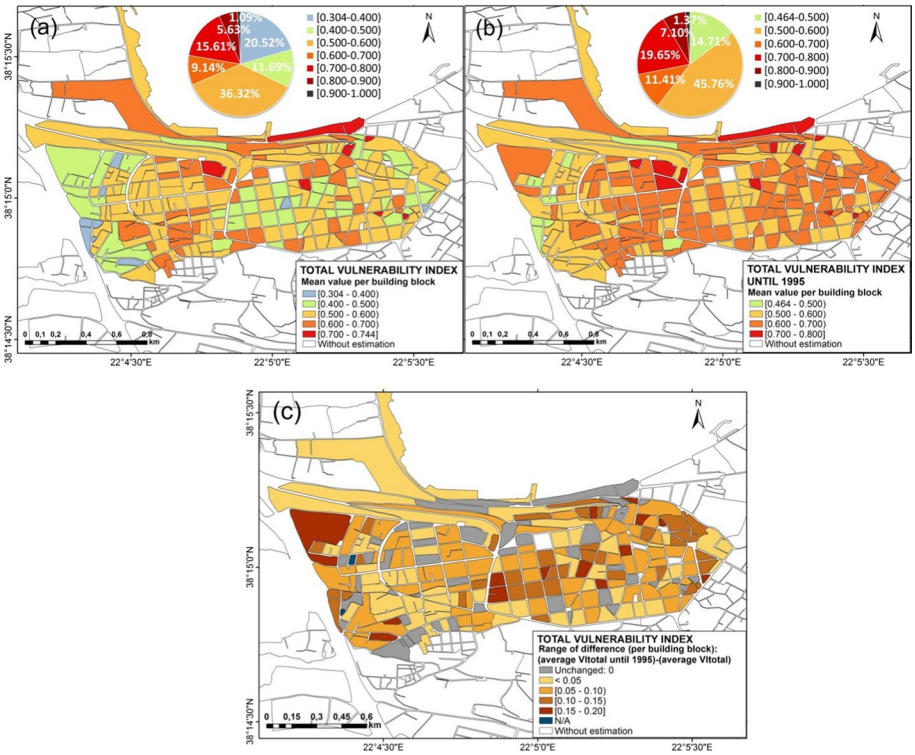

Fig. 11 The average $\bar{V}_I$ per building block and the respective percentages (embedded pie-charts): **a** for the current building stock, **b** for the era prior to the 1995 earthquake; **c** comparison between the two periods (unchanged: only buildings until 1995, N/A: only newly built buildings after 1995)

can be mainly found in the northern and partly in the central and southern parts of the city having an average $\bar{V}_I \geq 0.6$, while positive is the fact that the most vulnerable of them ($\bar{V}_I \geq 0.9$) are nowadays negligible (~ 1%), regarding adobe buildings in poor condition, or abandoned.

Figure 11b illustrates the distribution of the average $\bar{V}_I$ of buildings per block that were estimated to have been constructed until 1995. The respective building stock presents significantly higher vulnerability for this period. EXP-2016 corresponding to the period until 1995 (Fig. 11b) is composed of 1722 RC buildings (67.5% of the total sample until 1995), from which 8.9% and 58.6% are RC1 and RC2, respectively, and 828 URM buildings (32.5% of the aforementioned total sample). The average vulnerability ($\bar{V}_I$) of the two periods is compared in Fig. 11c in terms of $\bar{V}_{I_{diff}}$ ($\bar{V}_{I_{diff}} = \bar{V}_{I_{1995}} - \bar{V}_{I_{present}}$) demonstrating the enhancement of the current exposed assets thanks to rehabilitation after the 1995 earthquake.

4 Seismic risk assessment

Seismic risk in Aigion was assessed by combining the derived simulated ground motions and the structural vulnerability model. Equation (1) was applied to the EXP-2016 building stock for which the hazard analysis of the city was available (Fig. 6a), i.e. to 3059 inspected buildings of 217 city blocks, and an average value of synthetic PGA was thus assigned per building, for which the corresponding SI was attributed. Following the RiskUE-LM1 method, the mean damage grade, μ_D, of each building was then determined through the convolution of its SI and $\bar{V}_I$ value (Giovinazzi and Lagomarsino 2004),

$$\mu_D = 2.5 \cdot [1 + \tanh((SI + 6.25 \cdot \bar{V}_I - 13.1)/2.3)] \quad (2)$$

accompanied by the probability of occurrence, p_k per EMS-98 Damage Grade (DG, Table 5), which is described by the cumulative beta distribution function, P_β (Giovinazzi and Lagomarsino 2004):

$$\mu_D = \sum_{k=0}^{5} p_k \cdot k \quad (3)$$

$$p_k = P_\beta(k+1) - P_\beta(k) \quad (4)$$

The expected DGsare perceived as distinct variables, k, that range from 0 to 5 depending on the damage pattern: DG0-no damage, DG1-slight damage, DG2-moderate damage, DG3-heavy damage, DG4-very heavy damage, DG5-total collapse.

The two shape parameters r, t of the beta distribution and the μ_D are further associated by the form:

$$r = t \cdot \left(0.007 \cdot \mu_D^3 - 0.0525 \cdot \mu_D^2 + 0.2875 \cdot \mu_D\right) \quad (5)$$

in which a value of $t = 8$ was set (Giovinazzi and Lagomarsino 2004). By applying Eqs. (4) and (5), the probability of occurrence of each DG and the most probable DG per building were estimated. Moreover, the average value of μ_D per building block was calculated as a simplified illustration of the overall prevailing distribution. Hence, the probability of occurrence of the average DG and the most probable average DG on a building block scale were also determined (Eqs. 4, 5).

Table 5 Post-seismic usability according to the SER attributes and the herein damage classification of μ_D with respect to the considered range of the discrete EMS-98 DGs, in addition to their respesentative Damage Index (DI) that has been adopted

Usability (SER)	Damage characterization	DG (per EMS-98): μ_D (per RiskUE-LM1)	DI
Safe for use	No damage to Slight damage: No reduction of the seismic capacity	DG0: 0–0.5	0.5
		DG1: 0.5–1	
Unsafe for use	Moderate to Heavy damage: Need of repair before re-occupation	DG2: 1–2	2
Dangerous for use	Heavy to Very heavy damage: Prohibited approach-considerable dislocation, decision on possible repair or demolition	DG3: 2–3	3
		DG4: 3–4	
Collapsed	Partial/total collapse or demolished	DG5: 4–5	4

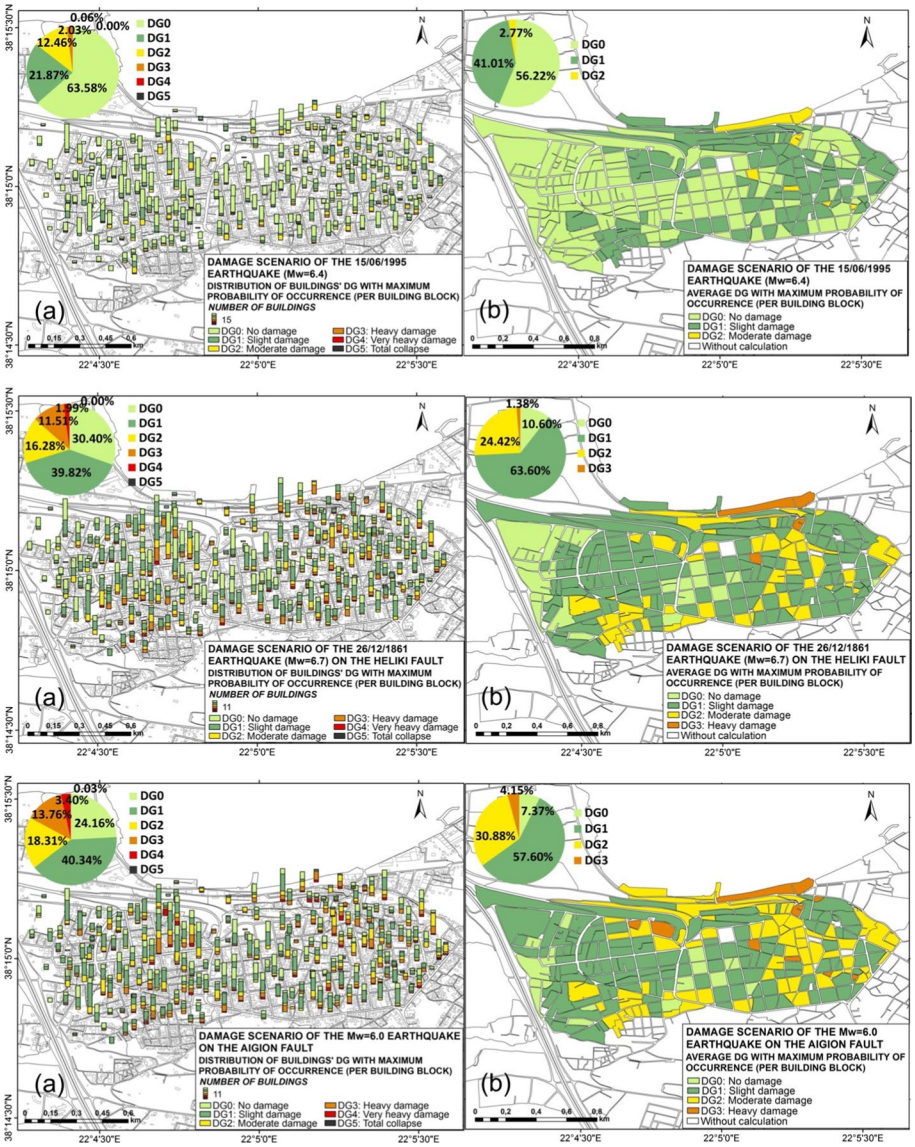

Fig. 12 Distribution of DGs with maximum probability of occurrence for seismic risk scenario 1 (top), scenario 2 (middle) and scenario 3 (bottom). **a** Number of buildings undergone a certain DG per building block; **b** averaged DG per building block. The embedded pie-charts present the corresponding percentages

4.1 Seismic risk scenarios

The damage potential for the three seismic scenarios in Aigion is presented in terms of DGs with maximum probability of occurrence on a building block scale (Fig. 12). Risk scenarios include all DGs, with the 15th June 1995 scenario (scenario 1) being the most favorable one. The *Mw*6.7 earthquake (scenario 2) on the EHF appears harmful,

while the most adverse one is the *Mw*6.0 earthquake on the AF (scenario 3), due to the proximity of the fault plane (see Fig. 5). The spatial distribution of the expected effects of our risk scenarios shows that damage is at most concentrated in the northeastern and in the southern part of the city, consistently with both the resulting distribution of soil amplification in the region (Fig. 5b) and increasing distance from the respective fault sources.

With regard to the scenario 1 (Fig. 12 Top), the distribution of DGs concern mainly DG0 with ~64%, DG1 with almost 22%, and DG2-DG3 with ~14% of the building stock. Scenarios 2 and 3 (Fig. 12 middle and bottom, respectively), on the other hand, indicate a significantly higher percentage of affected buildings with respect to scenario 1. In the case of the two latter scenarios, DG1 is almost similar about 40%, whereas DG2-DG3 and DG4 appear increased by about 2% and 1.4%, respectively, for the more adverse scenario 3 with respect to scenario 2. As for their DGs' maximum probability of occurrence shown in Fig. 13a, DG2 and especially DG3 indicate a considerably larger number and percentage for scenarios 2 and 3 with respect to scenario 1, DG4 appears with an increased difference up to 2–3% and DG5 up to about 1%, yet negligible in both cases. The prevailing average DG per block for scenarios 2 and 3 is DG1, with DG2 also yielding a high percentage of occurrence and with DG3 having a proportion of about 1.4% and 4.1%, respectively (Fig. 12b). Furthermore, the low proportion of DG4 and the negligible DG5 can presumably be attributed to the very few highly vulnerable buildings currently found in Aigion (Fig. 9a).

The comparative disaggregation of the results for the three seismic risk scenarios concerning buildings' response are presented in the histograms of Fig. 13. As far as the structural typology is concerned, vulnerable URM buildings were found to be most affected, exhibiting a significant percentage of DG3 and DG4 for scenarios 2 and 3 (Fig. 13b). URM-M6 type, though, was found to respond better, a fact that is attributed to the structures' enhancement by RC floors. Regarding RC buildings, consistently to the vulnerability per typology stemmed from the seismic design; RC1 type is found to exhibit a similar seismic behaviour to that of the vulnerable URM typologies (Fig. 13c). RC2 buildings are not subjected to a high DG, while RC3 typology is found to remain intact in all three cases. It is worth noting that for the adverse scenarios 2 and 3, vulnerability seems to play an important role, since buildings of higher vulnerability exhibit higher expected damage, while buildings of very low vulnerability remain intact in all cases (Fig. 13c).

Regarding the number of floors, the highest rate of DGs occurs mainly in the one- and two-storey URM and RC1 buildings characterized by higher vulnerability, while DGs gradually reduce for taller ones (Fig. 13d). This pattern is explained by the multitude of low-rise buildings in Aigion as well as to the fact that high-rise buildings, erected in the last decades, correspond mainly to RC2-RC3 typologies that exhibit in general lower vulnerability.

5 Comparison with observed damage

The robustness of the adopted methodology was tested against the observed damage pattern from the 15th June 1995 earthquake in the city of Aigion, that consists of attributes to RC and URM buildings assigned by the Sector for Earthquake Rehabilitation (SER; Fardis et al. 1999) post-seismic in situ inspections. This database includes usability

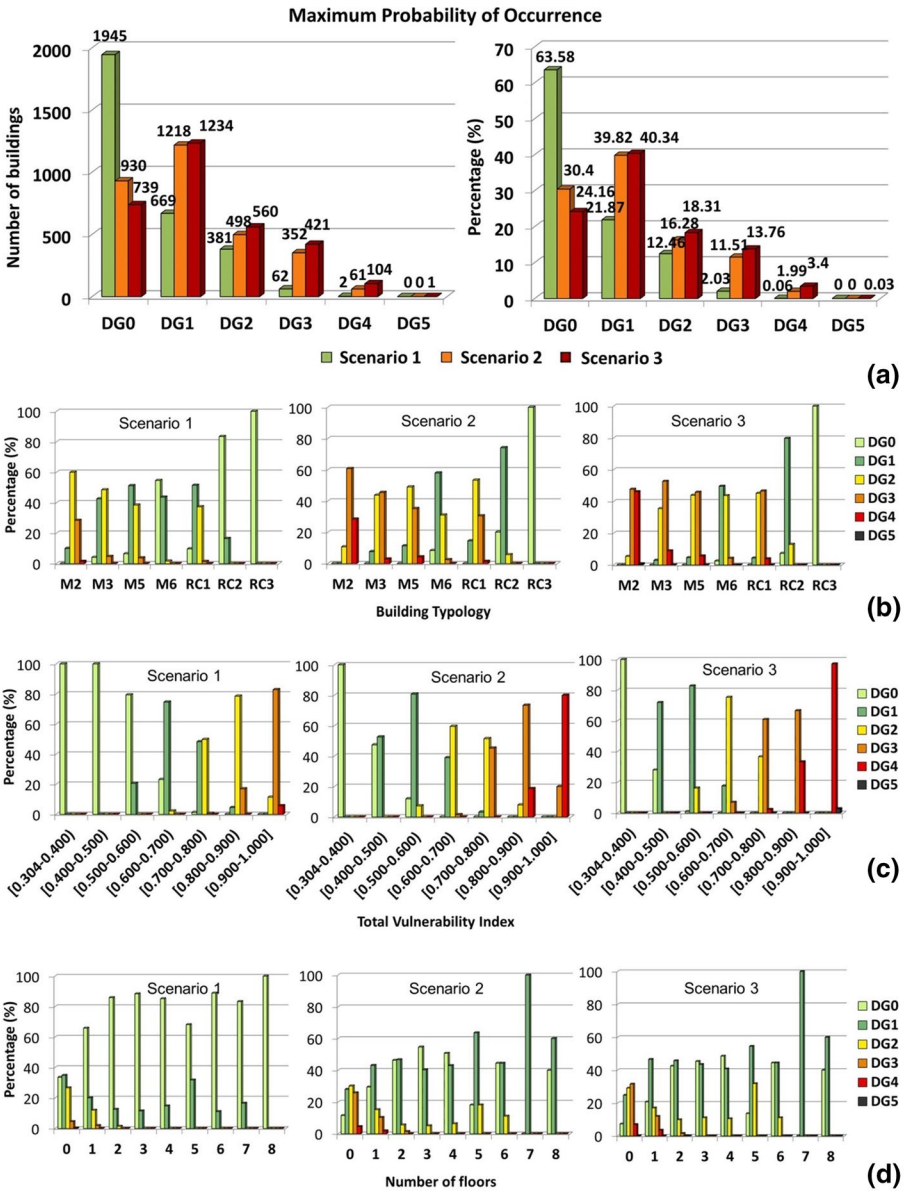

Fig. 13 **a** Summary of the expected buildings' DGs with maximum probability of occurrence for the three earthquake scenarios in terms of the number of buildings (left) and their percentage (right); DGs with respect to the percentage of maximum probability of occurrence regarding **b** the building typology, **c** the $\bar{V}_I$ of buildings, **d** the number of floors (the number 0 refers to the ground-floor buildings), for the three earthquake scenarios

characterization of the affected buildings with respect to their safety, following a simple coding protocol of three colors: "Green", "Yellow", and "Red" (Anagnostopoulos and Moretti 2008), as it is described in Table 5, in which an additional fourth damage color

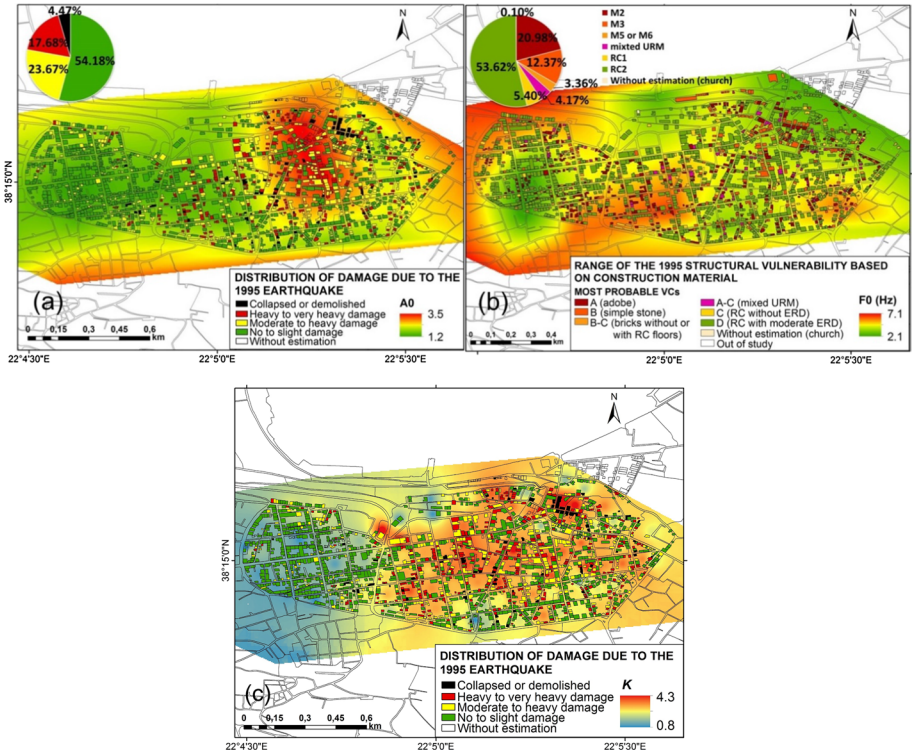

Fig. 14 Comparison **a** of the damage distribution of the 1995 Aigion earthquake (Fardis et al. 1999) to the simplified ambient noise HVSR amplification factor (A_0), and **b** of the 1995 building typology (Fardis et al. 1999) with the range of the most probable VCs based on construction material, to the ambient noise HVSR peak frequency (F_0); **c** spatial distribution of the index K and damage (Fardis et al. 1999) and for the 1995 earthquake

tag, "Black", is included to represent the collapsed buildings in Aigion due to the 1995 earthquake.

In order to compare the seismic risk scenario outcome with the real damage of 1995 in quantitative terms, both DGs and usability characterization had to have a common basis, therefore the qualitative damage was assessed assuming three terms, namely the discrete EMS-98 DGs, the mean damage grade (μ_D) of the RiskUE-LM1 methodology (Eq. 2), and the herein adopted Damage Index (DI), a compromise between μ_D and DG, as shown in Table 5. Accordingly, "color coding" was converted into discrete EMS-98 DGs and then μ_D was compared with DI per DG. For this purpose, the attributes proposed by Fardis et al. (1999) and Pomonis et al. (2014) for the URM and RC buildings in Aigion, respectively, were considered.

The analysis of the damage dataset revealed that ~54% of the inspected buildings were tagged as "Green" (DG0-DG1), ~24% as "Yellow" (DG2-DG3), ~18% as "Red" (DG3-DG4), while ~4% were partially or totally collapsed or had to be demolished due to irreparable damage (DG5) (Fig. 14a). Moderate-to-heavy (DG2-DG3) and very heavy damage (DG3-DG4) was mainly concentrated in the central and the eastern part of Aigion. This pattern is likely related to impacts from site effects and vulnerability.

Impact from site conditions is manifested in Fig. 14a which presents damage in juxtaposition to the soil response inferred by the ambient noise HVSR results. Specifically, largest effects at the eastern part of the city are related to both amplification (Fig. 14a) and high vulnerability (Fig. 14b), while damage in the central part of the city is compatible to the presence of numerous low-rise M2 and M3 buildings of high vulnerability. High soil peak frequencies, predominant in this area (Fig. 14b), possibly adversely interact with vulnerable adobe ground-floor structures found in this sector of the city.

In the waterfront area, several low-rise old vulnerable structures ($\bar{V}_I \geq 0.6$, Fig. 11) are located, which withstood shaking with some of them being still in use presently. Site amplification in this location is medium (~ 1.5–2, Fig. 14a), while predominant frequency is found about 2 Hz (T ~ 0.5 s) (Fig. 14b). The resistance of these buildings during the 1995 earthquake has been attributed to dampened ground motions in the soft and deep clayey deposits (Pomonis et al. 2014). Although more data are needed to investigate de-amplification effects, it is worth noting that spectral acceleration peak values of the 1995 near-field recordings are in the range T = 0.4–0.6 s, which interestingly are similar to the site's HVSR peak frequency and away from typical eigenperiods of such low constructions.

Given that seismic consequences are the combination of ground motion and structural vulnerability, coupling between structural damage and vulnerability is examined in reverse, to investigate the spatial distribution of strong ground motion during the 1995 earthquake as a site's response derivative. The term K is hence introduced as $K = \overline{DL}/\bar{V}_I^*$, where $\overline{DL}$ is the average value of μ_D (Eq. 3) per building block, determined in the case of the 1995 real damage distribution by assigning to each i_{th} damaged building the representative numerical value of damage index DI according to Table 5, and $\bar{V}_I^*$ is the respective estimated average typological VI (Giovinazzi and Lagomarsino 2004) of the n buildings per building block on the 1995 building stock (Fardis et al. 1999), therefore $\overline{DL} = \sum_{i=1}^{n} DIi/n$ and $\bar{V}_I^* = \sum_{i=1}^{n}[(V_I^*)_i/n]$, with $\bar{V}_I^* \in [0.4 - 0.8)$. K is applied as a preliminary qualitative index of consistency (low K) or inconsistency (high K) between observed damage and structural vulnerability, with higher values of K indicating possible site effects. Extreme deviation between the fraction's numerator ($\overline{DL}$) and denominator ($\bar{V}_I^*$) that might lead to artifacts by reversing the (low/high) polarity of K is absent from our dataset. Moreover, the calculation of the average K distribution is primarily intended to reduce any possible errors from the observed sample, therefore the concluded result can be considered an overall accurate depiction. However, further analysis with respect to the buildings' typological characteristics/modification scores and employment of more damage data are required in future investigations.

Nonetheless, in the case of the 1995 earthquake, the distribution of K (Fig. 14c) exhibits good correlation with the inferred soil response from ambient noise HVSR in terms of high A_0 (Fig. 14a) and high F_0 (Fig. 14b). Specifically, low K appears in particular at the western and partly at the northern part of the city, consistently with low site amplification (Fig. 14a), whereas high K is observed partly in the northeastern and the southern part of the city's center, in agreement with high A_0 (Fig. 14a) and high F_0, respectively (Fig. 14b).

A comparison between real and predicted damage from the 1995 simulated risk scenario 1 is shown in Fig. 15 per building block, in terms of DL, according to the assumed damage index (DI—Table 5) and to the predicted average value of μ_D (Eq. 3), respectively. The average damage distribution of the 1995 earthquake (Fig. 15a) is mostly characterized by moderate damage, while slight damage appears in particular at the western side and partly in the north of the city, consistent with the inferred distribution of undamaged

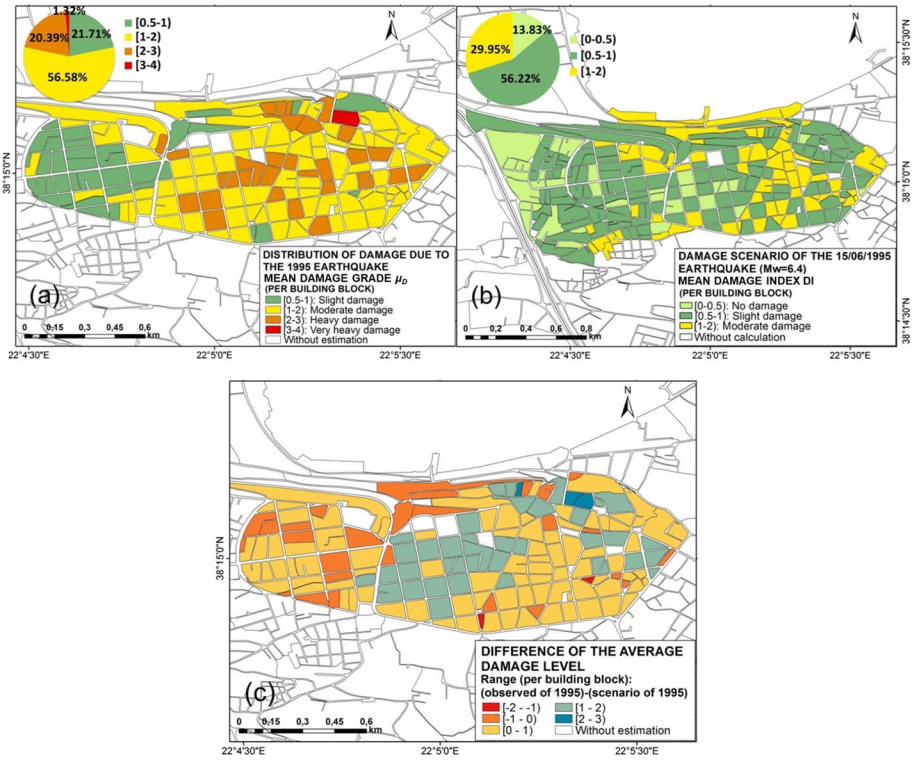

Fig. 15 Distribution of average damage level $\left(\overline{DL}\right)$ per building block in the city of Aigion, **a** due to the 1995 earthquake, and **b** regarding the respective simulated seismic scenario 1, in addition to **c** their comparative difference of $\left(\Delta\overline{DL}\right)_{1995}$ in the common studied area. The embedded pie-charts present the corresponding percentages

buildings from the corresponding seismic scenario 1 (Fig. 15b). Furthermore, the average percentage of heavy damage in the case of the 1995 earthquake occurs partly in the northeastern and southern part of the center, while little very heavy damage (1.3%) is locally concentrated in the northeast of the city. On the contrary, the respective simulated scenario appears generally more amenable than the real damage distribution of 1995, presenting moderate damage as the higher $\overline{DL}$ of the present building stock. The detailed comparison between the two resulting distributions for the common area of study is shown in Fig. 15c in terms of $(\Delta\overline{DL})_{1995}$, where $\left(\Delta\overline{DL}\right)_{1995} = \overline{DL}_{observed} - \overline{DL}_{scenario}$.

Enhancement of the seismic response of the recent building stock is observed mainly at the central and northeastern part of the city, due to rehabilitation and replacement of the heavily damaged and demolished buildings due to the 1995 earthquake with modern constructions, resulting in the reduction of the current city's vulnerability (Fig. 16). The comparison of structural vulnerability between the two observed samples, prior to (as per Fardis et al. 1999) and after 1995 (as per EXP-2016), displays a large proportion of the most vulnerable buildings, e.g. adobe URM, being replaced by newly built under high GSC

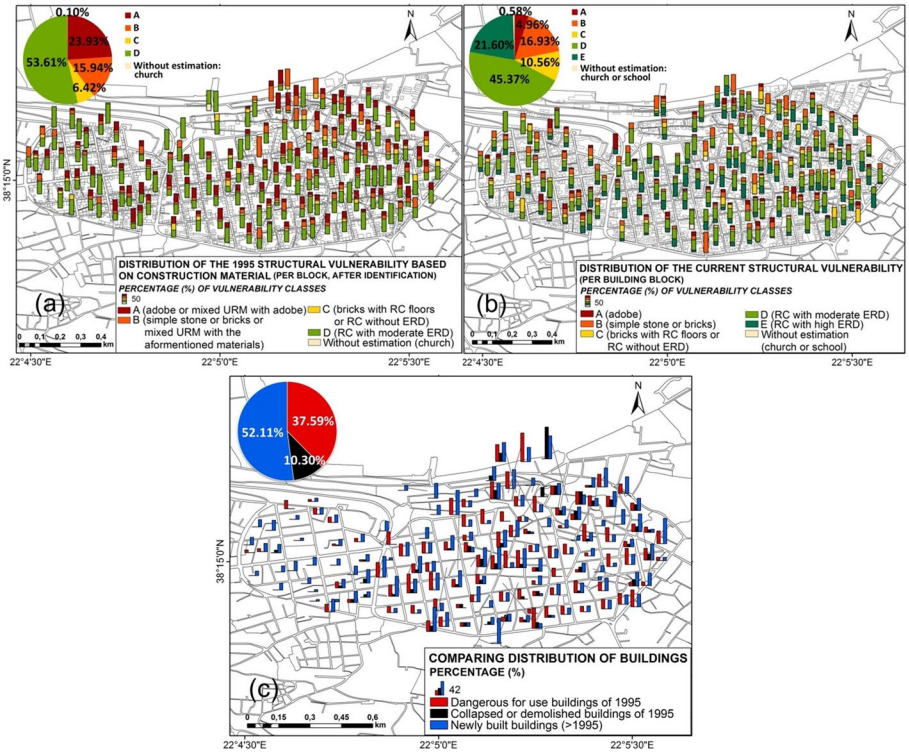

Fig. 16 Comparison of the estimated structural vulnerability per building block in Aigion, **a** for the 1995 period, based on the construction material characterization of Fardis et al. (1999), and **b** for the EXP-2016, in the common studied area. **c** Distribution of RC3 structures (blue) built in substitution of the very heavily damaged (red) and collapsed/demolished (black) buildings of 1995. The embedded pie-charts denote the corresponding percentages

RC3 ones. Moreover, a significant percentage of the current inspected sample includes buildings undergone strengthening post-earthquake interventions.

On the other hand, sparse negative $\left(\Delta\overline{DL}\right)_{1995}$ values in Fig. 15c, implying for deteriorated effects, are partly ascribed to the difference between the multitude of the two exposure models of the city's building stock, since EXP-2016 in the common studied area is found to be considerably larger. Few digitization uncertainties concerning location of buildings included in the database of Fardis et al. (1999) were treated according to the EPANTYK (2009) observations and the herein attributes, described above. It should be noted though that overstrength and actual seismic performance out of the typological boundaries of individual structures should not be neglected when simulated versus observed damage is studied.

6 Summary and conclusions

Devastating earthquakes produce painful lessons learned in terms of loss of human lives, property and societal disruption. However, "lessons learned" is often a vision rather than the reality, since this usually lacks incorporation of new knowledge in the risk assessment and the crisis management procedures. Hence, the latter are blind in the absence of tailored approaches, which are recognized to essentially support stakeholders making the right decisions and taking appropriate measures throughout potential crises.

In this respect, we elaborate a comprehensive physical seismic risk analysis in Aigion on a building block scale, taking into account (a) three selected hazardous fault sources, (b) site amplification approximated by simplified ambient noise HVSR curves, (c) realistic ground motion synthetics generated by applying the EXSIM stochastic finite-fault scheme, (d) the city's detailed exposure model, (e) real damage from the most recent devastating earthquake on 15th June 1995 (Mw6.4). The main outcome of our effort can be summarized as following.

The stochastic finite-fault scheme considered to simulate strong ground motions from the selected earthquake scenarios and the way it was applied was proven overall successful compared with the available real recordings. All damage grades (DG0-DG5) were found to be expected, with the most common DGs ranging from DG0 to DG3. In a spatial sense, the simulated risk scenarios display higher damage in the northeastern and to a lesser extend in the southern part of the city, consistently with the deduced HVSR amplification factors and also with the concentration of higher structural vulnerability. Scenario 3 on the closest AF, appears to be the most adverse one. The comparison of the simulated with the real damage of the 1995 earthquake demonstrated a compatible spatial distribution, although the potential impact appears to be significantly reduced when the current (EXP-2016) building stock is considered. Estimated consequences are adverse mainly because of old low-rise URM buildings and RC buildings without ERD, while the enhanced M6 type constructions and tall RC buildings with ERD are expected to exhibit better response. New RC buildings constructed according to the more rigorous provisions of the 1995 GSC appear to remain intact in all scenarios.

One of the most difficult tasks in scenario based seismic risk modelling is the nature and treatment of uncertainty and natural variability of the input and output parameters (e.g. Fäh et al. 2000). Oliveira (2008) outlines the main sources of epistemic and aleatory uncertainties in scenario-based seismic risk assessment (e.g. Kazantzidou-Firtinidou et al. 2018), as due to the seismic source, wave attenuation, site effect, buildings taxonomy, vulnerability, inventory, and methodology, together with possibilities to reduce each one of them. In the present case, uncertainties (epistemic) arise due to the fact that near-fault effects within the zone of permanent deformation could not be taken into account. Although such effects are most probable to occur during future earthquakes close to Aigion, they are difficult to be predicted as they depend on the details of the source process, which is not known a priori. Good knowledge of the seismotectonic environment allowed for the selection of specific faults and the definition of their geometry and kinematics, what reduced aleatory biases of the seismic hazard analysis. Moreover, the HVSR may underestimate actual site amplifications during strong ground motion, while aleatory uncertainties due to this method are related to the quality of measurements. Reduction of these uncertainties could be achieved, respectively, through the implementation of semi-analytical simulation methods (e.g. Roumelioti et al. 2003a, b; Graves and Pitarka 2015; Mavroeidis et al. 2018) and through the employment of more dense ambient noise measurements, as well as

existing (e.g. Apostolidis et al. 2006), with new geotechnical-geophysical data in the future Moreover, epistemic uncertainties related to the implementation of the empirical Eq. (1) for converting synthetic PGA into MMI are believed to have been excluded by calibration with other studies in Aigion.

As far as the epistemic uncertainties related to the estimation of the structural vulnerability, they are acknowledged within the probability and plausibility range of the vulnerability index inherently incorporated into the methodology applied. For illustration purposes and in order to render the results exploitable for disaster management purposes, a deterministic presentation of the results has been decided. In this respect, earthquake damage is represented herein by the most probable values. Parametric sensitivity and uncertainty evaluation is a future task by implementation of a logic tree scheme (e.g. Michel et al. 2017).

The major advantage of our work is that our methods were validated against existing, region-specific data before "blind'' ground motion predictions. Although a direct association between the probabilistic and deterministic outcome is not possible, it is worth noting that common finding in the examined scenarios is the exceedance of the "effective" design probabilistic PGA value of 0.24 g for a return period of 475 years (EAK-2000 2003). This is consistent with recorded near-field ground motions which exceeded the probabilistic predictions, such as in the cases of other strong earthquakes in the Greek territory, e.g. Lefkada 2003 (Gazetas 2004), Cephalonia 2014 (Kassaras et al. 2017) and elsewhere (Iervolino et al. 2017). Nevertheless, in case of realization of the scenario ground motions, the building stock of Aigion is found capable to withstand the shaking.

Future enhancement of the presented risk assessment regards the implementation of worst-case scenarios through a hazard disaggregation procedure so as to account for probabilities as in the probabilistic approach (PSHA) (e.g. Klügel 2007). The inclusion of temporal constraints of strong earthquakes occurrence on faults nearby the city should add to the applicability of the proposed seismic risk assessment towards preparedness and mitigation purposes. In this respect, modern methodologies using seismicity and strain rates estimates (Console et al. 2013; Durand et al. 2017) could be proven effective for modelling the probabilistic hazard from the complex fault system in the W. Corinth Gulf. Moreover, taking into account the building/soil frequency ratio (Salameh et al. 2017) could add to the reliability of the obtained vulnerability model in the future. Although fragility curves representative of part of the building stock in Aigion exist in the literature, their implementation is considered as a rough approximation since these are correlated with more sophisticated parameters apart from the PGA, i.e. spectral acceleration, spectral displacement, Arias intensity, which are not applied herein. Contrary, the development of representative fragility curves directly for the building stock of the area is recommended using the outcome of this work and further future enhancements outlined above. The implementation of empirical damage functions for the establishment of an integrated loss estimation model (e.g. Dolce et al. 2006; Karakostas et al. 2012; Silva et al. 2014) is also envisaged.

Even open to improvements, the outcome of this research is considered exploitable from stakeholders, and also promising for setting-up a future Rapid Risk Assessment (RRA) deployment in Aigion, provided the area's earthquake monitoring by modern networks. Furthermore, it could serve as risk assessment at sub-national level to the #1313/2013/EU Proposal for a Decision of the European Parliament and of the Council amending Decision on a Union Civil Protection Mechanism, which aims at strengthening the effectiveness of prevention action as part of a univocal disaster risk management cycle of the member states.

Acknowledgements We would like to acknowledge D. Kalantoni, N. Sakellariou, A. Karakonstantis, M. Machaira, S. Giannaraki, A. Makris, T. Aspiotis, S. Mourloukos, P. Stoumpos, Ch. Tsimi, K. Makropoulos for their valuable help and useful discussions that greatly contributed in the current research. We are also indebted to F. Karantoni for providing the vector damage data set of the 1995 Aigion earthquake. This work was partially supported by the ASPIS-KRIPIS (MIS-448326) research project. Figures 1, 3 and 5 were produced using GMT (Wessel and Smith 1991). Waveform data were processed using SAC2000 (Goldstein et al. 2003).

References

Albini P, Rovida A, Scotti O, Lyon-Caen H (2017) Large eighteenth–nineteenth century earthquakes in western Gulf of Corinth with reappraised size and location. Bull Seismol Soc Am 107(4):1663–1687

Anagnostopoulos S, Moretti M (2008) Post-earthquake emergency assessment of building damage, safety and usability—part 1: technical issues. Soil Dyn Earthq Eng 28:223–232

Apostolidis PI, Raptakis DG, Pandi KK, Manakou MV, Pitilakis KD (2006) Definition of subsoil structure and preliminary ground response in Aigion city (Greece) using microtremor and earthquakes. Soil Dyn Earthq Eng 26:922–940

Armijo R, Meyer B, King GCP, Rigo A, Papanastassiou D (1996) Quaternary evolution of the Corinth Rift and its implications for the Late Cenozoic evolution of the Aegean. Geophys J Int 126(1):11–53

ASPIS-KRIPIS (2015) Infrastructure upgrade for seismic protection of the country and strengthen service excellence through action, Project MIS-448326, implemented under the action. Development Proposals for Research Bodies-ASPIS-KRIPIS **(in Greek)**

Atkinson GM, Boore DM (1990) Recent trends in ground motion and spectral response relations for North America. Earthq Spectra 6:15–36

Atkinson GM, Boore DM (1995) Ground-motion relations for eastern North America. Bull Seismol Soc Am 85(1):17–30

Avallone A, Briole P, Agatza-Balodimou AM, Billiris H, Charade O, Mitsakaki C, Nercessian A, Papazissi K, Paradissis D, Veis G (2004) Analysis of eleven years of deformation measured by GPS in the Corinth Rift Laboratory area. C R Geosci 336:301–311

Bell RE, McNeill LC, Henstock TJ, Bull JM (2011) Comparing extension on multiple and depth scales in the Corinth Rift, Central Greece. Geophys J Int 186:463–470

Beresnev IA, Atkinson GM (1999) Generic finite-fault model for ground-motion prediction in eastern North America. Bull Seismol Soc Am 89(3):608–625

Bernard P, Briole P, Meyer B, Lyon-Caen H, Gomez J-M, Tiberi C, Berge C, Cattin R, Hatzfeld D, Lachet C, Lebrun B, Deschamps A, Courboulex F, Larroque C, Rigo A, Massonnet D, Papadimitriou P, Kassaras J, Diagourtas D, Makropoulos K, Veis G, Papazisi E, Mitsakaki C, Karakostas V, Papadimitriou E, Papanastassiou D, Chouliaras M, Stavrakakis G (1997) The Ms = 6.2, June 15, 1995 Aigion earthquake (Greece): evidence for low angle normal faulting in the Corinth rift. J Seismol 1:131–150

Bernard P, Lyon-Caen H, Briole P, Deschamps A, Boudin F, Makropoulos K, Papadimitriou P, Lemeille F, Patau G, Billiris H, Paradissis D, Papazissi K, Castarède H, Charade O, Nercessian A, Avallone A, Pacchiani F, Zahradnik J, Sacks S, Linde A (2006) Seismicity, deformation and seismic hazard in the western rift of Corinth: new insights from the Corinth Rift Laboratory (CRL). Tectonophysics 426:7–30

Boatwright J, Choy GL (1992) Acceleration source spectra anticipated for large earthquakes in Northeastern North America. Bull Seismol Soc Am 82(2):660–682

Bonnefoy-Claudet S, Cornou C, Bard P-Y, Cotton F, Moczo P, Kristek J, Fah D (2006) H/V ratio: a tool for site effects evaluation: results from 1-D noise simulations. Geophys J Int 167:827–837

Boore DM (1984) Use of seismoscope records to determine M_L and peak velocities. Bull Seismol Soc Am 74(1):315–324

Boore DM (1996) SMSIM—Fortran programs for simulating ground motions from earthquakes: Version 1.0. U.S Department of the Interior. US Geological Survey Open-File Report 96-80-A and 96-80-B, pp 73

Boore DM (2009) Comparing stochastic point-source and finite-source ground-motion simulations: SMSIM and EXSIM. Bull Seismol Soc Am 99(6):3202–3216

Boore DM, Atkinson GM (1987) Stochastic prediction of ground motion and spectral response parameters at hard-rock sites in eastern North America. Bull Seismol Soc Am 77(2):440–467

Brune JN (1970) Tectonic stress and the spectra of seismic shear waves from earthquakes. J Geophys Res 75(26):4997–5009
CAPRA, Probabilistic Risk Assessment Program. https://www.ecapra.org/. Accessed 22 May 2018
Chouliaras G, Kassaras I, Kapetanidis V, Petrou P, Drakatos G (2015) Seismotectonic analysis of the 2013 seismic sequence at the western Corinth Rift. J Geodyn 90:42–57
Console R, Falcone G, Karakostas V, Murru M, Papadimitriou E, Rhoades D (2013) Renewal models and coseismic stress transfer in the Corinth Gulf, Greece, fault system. J Geophys Res 118:3655–3673
Dolce M, Kappos A, Masi A, Penelis G, Vona M (2006) Vulnerability assessment and earthquake damage scenarios of the building stock of Potenza (S Italy) using Italian and Greek methodologies. Eng Struct 28:357–371
Douglas J, Monfort Climent D, Negulescu C, Roullé A, Sedan O (2015) Limits on the potential accuracy of earthquake risk evaluations using the L'Aquila (Italy) earthquake as an example. Ann Geophys 58(2):S0214. https://doi.org/10.4401/ag-6651
Doutsos T, Poulimenos G (1992) Geometry and kinematics of active faults and their seismotectonic significance in the western Corinth-Patras rift (Greece). J Struct Geol 14(6):689–699
Durand V, Hok S, Boiselet A, Bernard P, Scotti O (2017) Dynamic rupture simulations on a fault network in the Corinth Rift. Geophys J Int 208:1611–1622
EAK-2000 (2003) Greek National Building Code, earthquake protection and planning organization of Greece (OASP). EPPO Publications, Athens
Earthquake Protection and Prevention Organization-Institute of Engineering Seismology and Earthquake Engineering (EPPO-ITSAK). http://www.itsak.gr/en/main. Accessed 30 May 2018
EPANTYK (2009) Development of GIS software for the representation of the structural wealth of the municipalities of the country and of its structural vulnerability in buildings block level. YP.ES.A, H.D, KEDKE, TEE, pp 39 **(in Greek)**
ESD-European Strong-motion Database. http://www.isesd.hi.is/ESD_Local/frameset.htm. Accessed 30 May 2018
Fäh D, Bachmann H, Bay F, Becker A, Giardini D, Huggenberger P, Kind F, Lang K,Mayer-Rosa D, Noack T, Sellami S, Wenk T (2000) Earthquake scenarios for Switzerland. In: Proc XII world conference on earthquake engineering, New Zealand, Feb 2000, Paper No. 205
Fardis MN, Karantoni FV, Kosmopoulos A (1999) Statistical study of damage due to Aegion earthquake of 15-6-95. Final Report to Earthquake Planning and Protection Organization, University of Patras, Department of Civil Engineering, Division of Construction Engineering, Patras, July **(in Greek)**
Ganas A, Oikonomou IA, Tsimi C (2013) NOAfaults: a digital database for active faults in Greece. In: Bulletin of the Geological Society of Greece, Proceedings of the 13th International Congress, Chania, Sept. 2013, vol XLVII, no 2, pp 518–530
Gazetas G (2004) Geotechnical aspects of the Ms6.4 Lefkas Island, Greece, 2003 earthquake: preliminary assessment. In: Proceedings of the 5th international conference on case histories in geotechnical engineering, 13–17 April 2004, NY, paper No 13
Geodynamics Institute-National Observatory of Athens (GI-NOA). www.gein.noa.gr. Accessed 30 May 2018
Giovinazzi S, Lagomarsino S (2004) A macroseismic method for the vulnerability assessment of buildings. In: Proceedings of the 13th WCEE, Vancouver, BC, Canada, August 1–6, paper No 896
Godano M, Deschamps A, Lambotte S, Lyon-Caen H, Bernard P, Pacchiani F (2014) Focal mechanisms of earthquake multiplets in the western part of the Corinth Rift (Greece): influence of the velocity model and constraints on the geometry of the active faults. Geophys J Int 197:1660–1680
Goldstein P, Dodge D, Firpo M, Minner L (2003) SAC2000: signal processing and analysis tools for seismologists and engineers. In: The IASPEI international handbook of earthquake and engineering seismology. WHK Academic Press, London. http://dx.doi.org/10.1016/S0074-6142(03)80284-X
Graves R, Pitarka A (2015) Refinements to the Graves and Pitarka (2010) broadband ground motion simulation method. Seismol Res Lett 86:75–80
Greek government gazette 160/A (1959) Greek Antiseismic Regulation (R.D 19/26 February 1959) and Concrete Regulation—approved trends method (R.D 18-12-1954). Official Government Gazette 160/A
Grünthal G (1998) European Macroseismic Scale 1998 Cahiers du Centre Européen de Géodynamique et de Séismologie. Luxembourg 15:1–99
Hatzfeld D, Karakostas V, Ziazia M, Kassaras I, Papadimitriou E, Makropoulos K, Voulgaris N, Papaioannou C (2000) Microseismicity and faulting geometry in the Gulf of Corinth (Greece). Geophys J Int 141:438–456
Hatzidimitriou PM (1993) Attenuation of coda waves in northern Greece. Pure appl Geophys 140(1):63–78
Hatzidimitriou PM (1995) S-wave attenuation in the crust in northern Greece. Bull Seismol Soc Am 85(5):1381–1387

Iervolino I, Baltzopoulos G, Chioccarelli E, Suzuki A (2017) Seismic actions on structures in the near-source region of the 2016 central Italy sequence. Bull Earthq Eng. https://doi.org/10.1007/s10518-017-0295-3

Karakostas C, Lekidis V, Kappos A, Panagopoulos G, Kontoes C, Keramitsoglou I (2012) Evaluation of seismic vulnerability of buildings in Athens and L'Aquila in the framework of the MASSIVE seismic mitigation system. In: Proceedings of the 15th WCEE, LISBOA

Kassaras I, Kalantoni D, Benetatos C, Kaviris G, Michalaki K, Sakellariou N, Makropoulos K (2015) Seismic damage scenarios in Lefkas old town (W Greece). Bull Earthq Eng. https://doi.org/10.1007/s10518-015-9789-z

Kassaras I, Papadimitriou P, Kapetanidis V, Voulgaris N (2017) Seismic site characterization at the western Cephalonia Island in the aftermath of the 2014 earthquake series. Int J Geo-Eng. https://doi.org/10.1186/s40703-017-0045-z

Kassaras I, Kazantzidou-Firtinidou D, Ganas A, Kapetanidis V, Tsimi C, Valkaniotis S, Sakellariou N, Mourloukos S (2018) Seismic risk and loss assessment for Kalamata (SW Peloponnese, Greece) from neighbouring shallow sources. Bolletino di Geofisica Teorica e Applicata 59(1):1–26

Kazantzidou-Firtinidou D, Kassaras I, Ganas A (2018) Empirical seismic vulnerability, deterministic risk and monetary loss assessment in Fira (Santorini, Greece). Nat Hazards. https://doi.org/10.1007/s11069-018-3350-8

Klügel JU (2007) Comment on "Why do modern probabilistic seismic-hazard analyses often lead to increased hazard estimates" by J Bommer and NA Abrahamson. Bull Seismol Soc Am 97:2198–2207

Konno K, Ohmachi T (1998) Ground-motion characteristics estimated from spectral ratio between horizontal and vertical components of microtremor. Bull Seismol Soc Am 88(1):228–241

Lekidis VA, Karakostas CZ, Dimitriu PP, Margaris BN, Kalogeras I, Theodulidis N (1999) The Aigio (Greece) seismic sequence of June 1995: seismological, strong motion data and effects of the earthquakes on structures. J Earthq Eng 3(3):349–380

Makropoulos K, Kaviris G, Kouskouna V (2012) An updated and extended earthquake catalogue for Greece and adjacent areas since 1900. Nat Hazards Earth Syst Sci 12:1425–1450

Margaris BN, Boore DM (1998) Determination of $\Delta\sigma$ and κ_0 from response spectra of large earthquakes in Greece. Bull Seismol Soc Am 88(1):170–182

Mavroeidis GP, Ding Y, Moharrami N (2018) Revisiting the 1995 *MW*6.4 Aigion, Greece, earthquake: simulation of broadband strong ground motion and site response analysis. Soil Dyn Earthq Eng 104:156–173

McNeill LC, Collier RE, De Martini PM, Pantosti D, D'Addezio G (2005) Recent history of the Eastern Eliki Fault, Gulf of Corinth: geomorphology, palaeoseismology and impact on palaeoenvironments. Geophys J Int 161(1):154–166

McNeill LC, Cotterill CJ, Bull JM, Henstock TJ, Bell R, Stefatos A (2007) Geometry and slip rate of the Aigion fault, a young normal fault system in the western Gulf of Corinth. Geology 35(4):355–358

Micarelli L, Moretti I, Jaubert M, Moulouel H (2006) Fracture analysis in the south-western Corinth rift (Greece) and implications on fault hydraulic behavior. Tectonophysics 426:31–59

Michel C, Fah D, Lestuzzi P, Hannewald P, Husen S (2017) Probabilistic mechanics-based loss scenarios for school buildings in Basel. Bull Earthq Eng 15(4):1471–1496

Milutinovic ZV, Trendafiloski GS (2003) An advanced approach to earthquake risk scenarios with applications to different European towns. Report WP4: Vulnerability of current buildings, RISK-UE, EC, Brussels, pp 109

Motazedian D, Atkinson GM (2005) Stochastic finite-fault modeling based on a dynamic corner frequency. Bull Seismol Soc Am 95(3):995–1010

Musson RMW, Grünthal G, Stucchi M (2010) The comparison of macroseismic intensity scales. J Seismol 14:413–428

Nakamura Y (1989) A method for dynamic characteristics estimation of subsurface using microtremor on the ground surface. Q Rep Railw Tech Res Inst 30(1):25–33

Oliveira CS (2008) Lisbon earthquake scenarios: a review on uncertainties, from earthquake source to vulnerability modelling. Soil Dyn Earthq Eng 28:890–913

OpenQuake. https://platform.openquake.org/. Accessed 22 May 2018

Palyvos N, Pantosti D, De Martini PM, Lemeille F, Sorel D, Pavlopoulos K (2005) The Aigion-Neos Erineos coastal normal fault system (western Corinth Gulf Rift, Greece): geomorphological signature, recent earthquake history, and evolution. J Geophys Res. https://doi.org/10.1029/2004JB003165

Pantosti D, De Martini PM, Koukouvelas I, Stamatopoulos L, Palyvos N, Pucci S, Lemeille F, Pavlides S (2004) Palaeoseismological investigations of the Aigion Fault (Gulf of Corinth, Greece). C R Geosci 336(4–5):335–342

Papadopoulos G (2003) Tsunami hazard in the Eastern Mediterranean: strong earthquakes and tsunamis in the Corinth Gulf, Central Greece. Nat Hazards 29:437–464

Papaioannou CA (2014) The Aigio (C Greece) *Mw*5.0 earthquake of November 7, 2014 Brief information on active tectonics, seismicity and analysis of the acceleration records. Ministry of Infrastructures Transportation and Networks, Earthquake Planning and Protection Organization, Research Unit "ITSAK", Thessaloniki-Greece, pp 1–17

Papazachos B, Papazachou C (1997) The earthquakes of Greece. Editions Ziti, Thessaloniki

Papazachos BC, Papaioannou CA, Papazachos CB, Savvaidis AS (1997) Atlas of isoseismal maps for strong shallow earthquakes in Greece and surrounding area (426 BC-1995). University of Thessaloniki, Geophysical Laboratory Publication, 4: pp 175

Pomonis A, Gaspari M, Karababa FS (2014) Seismic vulnerability assessment for buildings in Greece based on observed damage data sets. Bollettino di Geofisica Teorica ed Applicata 552:501–534

RASOR (Rapid Analysis And Spatialisation Of Risk). http://www.rasor-project.eu. Accessed 25 June 2018

Rodriguez VHS, Midorikawa S (2002) Applicability of the H/V spectral ratio of microtremors in assessing site effects on seismic motion. Earthq Eng Struct Dyn 31:261–279

Roumelioti Z, Kiratzi A, Theodoulidis N, Kalogeras I, Stavrakakis G (2003a) Rupture directivity during the September 7, 1999 (*Mw* 5.9) Athens (Greece) earthquake inferred from forward modeling of strong ground motion. Pure Appl Geophys 160:2301–2318

Roumelioti Z, Dreger D, Kiratzi A, Theodoulidis N (2003b) Slip distribution of the 7 September 1999 Athens earthquake inferred from an empirical Green's function study. Bull Seismol Soc Am 93(2):775–782

Salameh C, Bard P-Y, Guillier B, Harb J, Cornou C, Gérard J, Almakari M (2017) Using ambient vibration measurements for risk assessment at an urban scale: from numerical proof of concept to Beirut case study (Lebanon). Earth Planets Space 69(60):1–17

Schmidt J (1879) Studien uber Erdbeben Carl Schottze. Leipzig, pp 68–83

SESAME (2005) Guidelines for the implementation of the H/V spectral ratio technique on ambient vibrations-measurements, processing and interpretations. SESAME European research project EVG1-CT-2000–00026, D23.12

Shebalin NV (1974) Atlas of isoseismal maps Part III UNDP/UNESCO. Survey of the Seismicity of the Balkan Region, Skopje, 275 maps

Silva V, Crowley H, Varum H, Pinho R (2014) Seismic risk assessment for mainland Portugal. Bull Earthq Eng 13(2):429–457

Tomás A, Ródenas JL, García-Ayllón S (2017) Proposal for new values of behavior modifiers for seismic vulnerability evaluation of reinforced concrete buildings applied to Lorca (Spain) using damage data from the 2011 earthquake. Bull Earthq Eng 15(9):3943–3962. https://doi.org/10.1007/s10518-017-0100-3

Tselentis G-A, Danciu L (2008) Empirical relationships between modified Mercalli intensity and engineering ground-motion parameters in Greece. Bull Seismol Soc Am 98(4):1863–1875

Voulgaris N, Kassaras I, Papadimitriou P, Kaviris G, Makropoulos K, Diagourtas D, Pitilakis K (2010) HVSR method sensitivity investigation for the CORSSA array in W. Corinth gulf (Greece). 32nd General Assembly of the ESC 2010, Montpellier, France, 6–10 September 2010, Oral & Poster Abstracts: 207

Wells DL, Coppersmith KJ (1994) New empirical relationships among magnitude, rupture length, rupture width, rupture area, and surface displacement. Bull Seismol Soc Am 84(4):974–1002

Wessel P, Smith WHF (1991) Free software helps map and display data. EOS Trans Am Geophys Union 72(41):441–448